Palaeogeography, Palaeoclimatology, Palaeoecology 679 (2025) 113270

Contents lists available at ScienceDirect

Palaeogeography, Palaeoclimatology, Palaeoecology

journal homepage: www.elsevier.com/locate/palaeo

Intense continental weathering during the early Ediacaran; in the aftermath of the Marinoan snowball Earth

Yusuke Sawaki [a,*], Kota Namba [a], Takuya Aikawa [b], Miyuki Tahata [a], Takeshi Ohno [b], Tsuyoshi Komiya [a], Jian Han [c]

[a] Department of Earth Science and Astronomy, The University of Tokyo, 3-8-1 Komaba, Meguro-ku, Tokyo 153-8902, Japan
[b] Department of Chemistry, Faculty of Science, Gakushuin University, Mejiro 1-5-1, Toshima-ku, Tokyo 171-8588, Japan
[c] Shaanxi Key Laboratory of Early Life and Environments (SKLELE), State Key Laboratory of Continental Evolution and Early Life (SKLCEEL), Department of Geology, Northwest University, Xi'an, 710069, P.R. China

ARTICLE INFO

Editor: B Shen

Keywords:
Ediacaran period
Continental slope facies
Doushantuo Formation
$^{87}Sr/^{86}Sr$ excursion
Mo enrichment

ABSTRACT

The Ediacaran period witnessed one of the most significant episodes of biological evolution in Earth's history. To reconstruct the environmental changes during this period, researchers have employed multi-geochemical proxies from Ediacaran strata. Continental weathering exerts a major influence on seawater composition and the evolution of life, and its flux can be estimated using the $^{87}Sr/^{86}Sr$ ratio of carbonate rocks. The secular variation of Ediacaran marine $^{87}Sr/^{86}Sr$ composition has been primarily reconstructed from Ediacaran strata in South China. However, because existing $^{87}Sr/^{86}Sr$ data are derived from tidal flat to shelf margin settings, clarifying the $^{87}Sr/^{86}Sr$ ratios in more distal settings is essential for comprehensively tracking the $^{87}Sr/^{86}Sr$ composition of the open ocean. We conducted on-land drilling to collect Ediacaran sedimentary rocks from the Tianping and Siduping sections, both located in slope settings. SEM-EDS observations revealed that the carbonate rocks at these sections experienced dolomitization, clay mineral formation, and silicification during diagenesis. Clay mineral-free carbonate rocks exhibit positive La and Y anomalies, indicating deposition in an open marine environment. $^{87}Sr/^{86}Sr$ values in the basal Doushantuo Formation at the Tianping section decreased from approximately 0.709 to approximately 0.708. This highly radiogenic value following the Marinoan glaciation is a novel finding of this study and suggests an elevated continental weathering influx post-Marinoan glaciation. $^{87}Sr/^{86}Sr$ profiles at the Siduping section demonstrate that high $^{87}Sr/^{86}Sr$ ratios around the Shuram excursion are common features of carbonate rocks deposited in various settings at this time. Consequently, this study confirms that continental weathering was elevated at approximately 635 Ma, 580 Ma, and 560 Ma. These timings coincide with three intervals of Mo enrichment in euxinic shales. This supports the hypothesis that globally elevated rates of continental weathering were closely linked to ocean oxygenation events during the Ediacaran.

1. Introduction

The Ediacaran period (approximately 635–539 Ma) is characterized by several dramatic events, including ocean oxygenation episodes (e.g., Sahoo et al., 2016; Hardisty et al., 2017), continental breakup and collisions (Dalziel, 1991; Karlstrom et al., 2001; Squire et al., 2006), the diversification of metazoans (e.g., Brasier and Antcliffe, 2004), and significant perturbations in surface environments, as recorded by isotope proxies (e.g., Fike et al., 2006; Hurtgen et al., 2002; Sawaki et al., 2010a; Cui et al., 2021). The weathering influx from continents is considered to have a major influence on seawater composition and the evolution of life. In general, enhanced continental weathering leads to an increase in nutrient supply, promoting the proliferation of primary producers. The net burial of organic matter in sedimentary rocks creates an excess inventory of free oxygen, increasing the oxidation state of the ocean-atmosphere system (Garrels and Perry, 1974; Des Marais, 1994). The $^{87}Sr/^{86}Sr$ value of seawater primarily reflects a combination of hydrothermal and riverine inputs. Due to the substantial isotopic difference between these sources, the $^{87}Sr/^{86}Sr$ composition of carbonate rocks can track long-term changes in continental weathering influx relative to hydrothermal flux (e.g., Richter et al., 1992). Existing data from Ediacaran carbonate rocks indicate that continental weathering

* Corresponding author.
E-mail address: y-sawaki@g.ecc.u-tokyo.ac.jp (Y. Sawaki).

https://doi.org/10.1016/j.palaeo.2025.113270
Received 25 March 2025; Received in revised form 17 August 2025; Accepted 7 September 2025
Available online 8 September 2025
0031-0182/© 2025 The Authors. Published by Elsevier B.V. This is an open access article under the CC BY license (http://creativecommons.org/licenses/by/4.0/).

was elevated around approximately 580 Ma (Sawaki et al., 2010a) and approximately 560 Ma (Chen et al., 2022). The former is related to the Gaskiers glaciation, whereas the latter is contemporaneous with the so-called Shuram excursion, the largest carbonate carbon isotope ($\delta^{13}C_{carb}$) anomaly during the Ediacaran period.

The environment immediately following the Marinoan glaciation (approximately 643–635 Ma) has recently garnered significant attention. Deglacial intense continental weathering was proposed in the Snowball Earth hypothesis (e.g., Hoffman et al., 1998; Hoffman and Schrag, 2002). Within this hypothesis, the deposition of cap carbonate itself is considered evidence of intense continental weathering. Furthermore, under the concept of "plumeworld" (Shield, 2005), strong terrestrial meltwater influx after the Marinoan glaciation has been suggested by stable isotope signatures of cap carbonate, including Li, Ca, and Sr isotopes (e.g., Wei et al., 2019; Wang et al., 2023; Gan et al., 2024). However, the stable isotope signature of carbonate rocks depends on several parameters, such as the balance of influxes and outfluxes and isotopic fractionation between seawater and the solid phase. Consequently, the interpretation of stable isotopes is not straightforward, and existing data are not necessarily directly linked to enhanced continental weathering. Transient inputs of terrestrial meltwater and deglacial runoff were also suggested by high $^{87}Sr/^{86}Sr$ values in Marinoan cap carbonate (Liu et al., 2013, 2014; Wei et al., 2019). Conversely, previous studies have assumed that cap dolostones predominantly precipitated from meltwater. The high $^{87}Sr/^{86}Sr$ values might reflect a local and/or short-lived event, thus they appear insufficient as evidence of deglacial intense continental weathering on a global scale. It has been pointed out that the intensity of chemical weathering during cap carbonate deposition was weaker than that during the Marinoan glaciation (Huang et al., 2016; Li et al., 2020).

The fossiliferous Doushantuo Formation (Fm) in South China is a crucial Ediacaran sedimentary unit, providing a continuous oceanic record due to the successive occurrence of carbonate rocks. Its depositional setting ranges from shallow marine platforms to deep basins (Fig. 1). Previous studies have reported the secular variation of $^{87}Sr/^{86}Sr$ values using carbonate rocks from the Doushantuo Fm at the Three Gorges (Sawaki et al., 2010a), Wangjiapeng (Lan et al., 2019), Zhongling (Cui et al., 2015), Yangjiaping (Furuyama et al., 2016), and Weng'an sections (Fan et al., 2024). High $^{87}Sr/^{86}Sr$ values from phosphorites at the Weng'an section are attributed to the enhanced contribution of terrigenous materials to the local depositional environment (Fan et al., 2024), whereas the aforementioned four sections were located in the inner part of the basin (Fig. 1). Particularly for the lower Doushantuo Fm in these inner settings, a nonmarine environment has been proposed based on clay mineralogy (Bristow et al., 2009). Because existing $^{87}Sr/^{86}Sr$ data reported from South China are limited to these inner settings, clarifying the $^{87}Sr/^{86}Sr$ ratios in more distal settings is essential for comprehensively tracking surface environmental changes throughout the Ediacaran period.

Strontium isotopic signatures are susceptible to alteration. Therefore, we used drill-core samples unaffected by surficial alteration and oxidation processes, enabling us to generate highly continuous stratigraphic sections with centimeter-scale sampling resolution. This paper presents radiogenic strontium isotopic profiles at the Siduping and Tianping sections in South China, where Ediacaran sediments deposited in continental slope settings are well exposed. These newly obtained Sr isotopic profiles, combined with existing data, allow for a comprehensive reconstruction of oceanic environments during the Ediacaran.

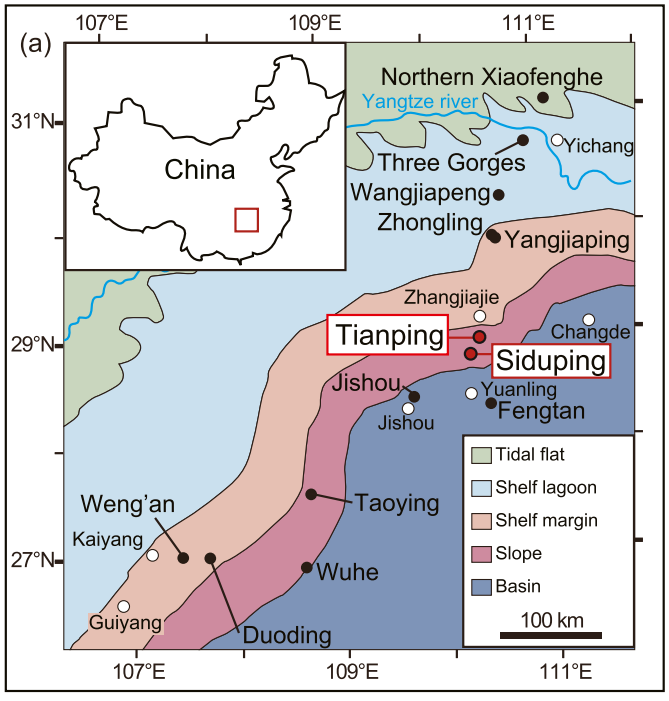

Fig. 1. (a) Simplified paleogeographic map around the Yangtze block through the Ediacaran period (modified from Jiang et al., 2011). The drilling core samples studied herein were collected at the Siduping and Tianping sections.

2. Geological outline

Neoproterozoic to Cambrian strata are widely distributed in South China (Fig. 1). Paleogeographic reconstructions around the Yangtze block indicate a southeast-facing Ediacaran Yangtze platform, encompassing marine settings ranging from the shallow marine shelf to deep basins (Jiang et al., 2007, 2011; Zhu et al., 2003, 2007a). This platform developed on the continental margin of the Yangtze block, which rifted off the Cathaysia block after approximately 800 Ma (Li et al., 1999; Wang and Li, 2003). Furthermore, these strata contain numerous fossils of eukaryotes and the earliest multicellular organisms, including animal embryos, sponges, algae, and acritarchs (e.g., Chen et al., 2002, 2014a, 2014b; Xiao et al., 1998, 2014a, 2014b; Yin et al., 2007; Zhou and Xiao, 2007). We conducted drilling at the Siduping and Tianping sections, both of which are considered to correspond to a continental slope setting based on paleogeographic reconstructions (Jiang et al., 2003, 2011).

2.1. *Siduping section*

Cryogenian to Cambrian sedimentary rocks are exposed in both the northwest and southeast parts of Siduping village due to the presence of a syncline. The sequence between the Nantuo Fm and Niutitang Fm crops out along a river in the southeastern part (Fig. 2). The Nantuo Fm is primarily composed of green diamictite, with its upper part including a 1 m-thick, coarse-grained, pyrite-bearing white sandstone layer. The Doushantuo Fm consists of the basal cap carbonate and interlayers of black shale and dolostone in its middle and upper parts. The cap carbonate is subdivided into three parts. The lower part is characterized by stromatactis structures, in which abundant organic matter and pyrite grains occur in frequently silicified cavities. The middle part comprises a bedded dolostone layer occasionally marked by tepee-like structures. The upper part includes bedded dolostones with very thin black shale layers.

The sequence overlying the cap carbonate exhibits slumping structures and black chert nodules and is subdivided into three parts: black shale-dominant, carbonate-dominant, and black shale-predominant, in ascending order. The lower part is mainly composed of black shale with interlayered discontinuous pyrite and siliceous nodules. The black shale layer near the base of the lower unit is characterized by elevated total organic carbon (TOC) concentrations, exceeding 4 wt% (Wang et al., 2016). Hawkins et al. (2017) documented the occurrence of *Hocosphaeridium anozos* approximately 40 m above the Doushantuo/Nantuo boundary. This fossil defines the upper acritarch biozone within the

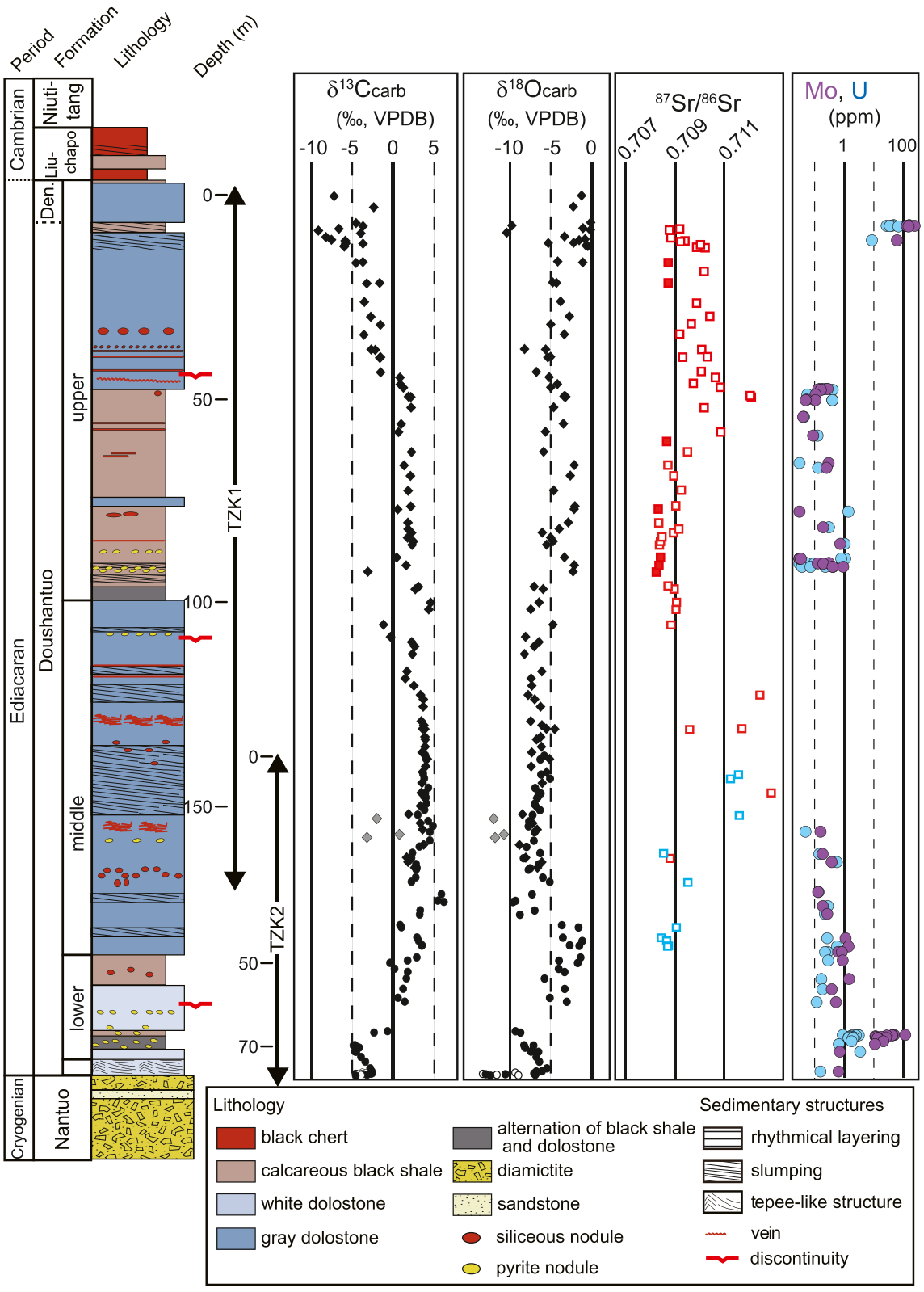

Fig. 2. Lithostratigraphy of the Siduping section from the late Cryogenian through the Ediacaran to the Cambrian. White rhomboids next to cap carbonates represent the isotopic data obtained from veins. Gray rhomboids in carbon and oxygen profiles signify data exhibiting a positive correlation in the $\delta^{13}C$–$\delta^{18}O$ cross-plot diagram (Fig. S2a) and are excluded from Figs. 9. Open symbols in the $^{87}Sr/^{86}Sr$ diagram indicate $^{87}Sr/^{86}Sr$ data with Mn/Sr ratios higher than 1 and/or Sr contents lower than 200 μg/g.

Doushantuo Fm and has been reported from Member 3 at the Three Gorges section (Xiao et al., 2014b). The middle part is dominated by carbonate rocks and is transected by numerous quartz veins, which may serve as a useful marker between the two sets of drill cores. The upper part consists of calcareous black shales and dolostones with siliceous and pyrite nodules. The 2 m-thick black shale layer near the top of the Doushantuo Fm is characterized by high abundances of TOC (Wang et al., 2016), similar to Member 4 of the Doushantuo Fm in other areas. Slump folds and discrete discontinuities indicate gravity-related mass movement and deposition at slope facies (Vernhet et al., 2006). Such structures are seen in many sequences of the Doushantuo Fm (Fig. S1).

The dolostone above the black shale may correspond to the Dengying Fm (Fig. 2), as carbonate rocks occur between Member 4 and the Precambrian/Cambrian (Pc/C) boundary in other sections of South China. The Liuchapo Fm contains two black chert layers with a thin black shale layer in the middle. The exact position of the Pc/C boundary at the Siduping section remains undetermined due to the lack of index fossils and chronological constraints.

We collected two sets of drilling core samples at the Siduping section. The first set was taken from just below the black chert layer in the Liuchapo Fm to the middle of the Doushantuo Fm (TZK1; Table S1). The second set was taken from the middle of the Doushantuo Fm to the uppermost part of the Nantuo Fm (TZK2; Table S2). We combined these two sets of drill cores using the key marker bed of dolostone transected by abundant silica veins, as described above (Fig. 2).

2.2. Tianping section

The Tianping section is located 40 km southwest of Zhangjiajie city. The Ediacaran to early Cambrian succession consists of the Nantuo, Doushantuo, Dengying, Liuchapo, and Niutitang formations, in ascending order (Fig. 3).

The Nantuo Fm is composed of diamictites interbedded with discontinuous mudstone and sandstone layers at various stratigraphic levels. The Doushantuo Fm comprises the basal cap carbonate and an upper alternation of black shale and dolostone, along with some limestone layers. The cap carbonate is primarily composed of an approximately 6 m-thick white dolostone and rests, with a sharp contact, on the Nantuo diamictite. The lower part of the cap carbonate displays highly disrupted, convoluted, and stromatactis structures with a high abundance of organic matter. Silicification along the rims of cavities and veins is also observed. Above the cap carbonate, the lower part of the Doushantuo Fm is dominated by black shale with dolostone layers. In the middle of the Doushantuo Fm, thick limestone layers with black siliceous nodules and slumping structures occur. The presence of slumping structures indicates deposition in a slope setting, supporting the conclusions of previous studies (e.g., Zhu et al., 2007a). Additionally, the upper Doushantuo Fm mainly consists of black shale with some limestone layers. Carbonate layers with abundant oolites at a height of 106 m indicate deposition in a shallow marine environment, possibly due to a lowering of the sea level. The boundary between the Doushantuo and Dengying formations is defined as the base of white bedded dolostones. The Dengying Fm at this section is relatively thin, approximately 55 m, compared with that in inner shelf settings such as the Three Gorges section (> 240 m; Zhao et al., 1988). The base of the black chert-dominant layer defines the boundary between the Dengying and Liuchapo formations. The Liuchapo Fm is approximately 15 m thick and comprises black chert with a distinct black shale layer in its middle part. The Niutitang Fm overlying the Liuchapo Fm predominantly comprises black shale with some limestone layers. Similar to the Siduping section, the Pc/C boundary at this section has not been fully constrained due to the lack of index fossils and chronological data. We collected a drill-core sample from the middle Doushantuo Fm to the Nantuo Fm (TZK3; Table S3) and outcrop samples from the Nantuo, Doushantuo, Dengying, and Niutitang formations (Table S4).

3. Analytical methods

Powdered samples were prepared from fresh-cut surfaces of the drill cores and outcrop samples using a micro-drill with a 3 mm bit. Sampling points were carefully selected in order to avoid contamination from visible veins. In addition to rare earth element (REE) abundance and Sr isotope analyses, we determined carbon and oxygen isotope ratios of carbonate fraction ($\delta^{13}C_{carb}$ and $\delta^{18}O_{carb}$) and molybdenum (Mo) and uranium (U) abundances of carbonate rocks and shales.

3.1. Carbon and oxygen isotope

A standard acid digestion technique was used in extracting carbon and oxygen from carbonate (Wachter and Hayes, 1985). The powdered samples, ~0.5 mg for carbonate samples and ~ 1 mg for calcareous black shale, were reacted with >100 % phosphoric acid at 72 °C for over 6 h to release CO_2 within sealed test tubes. After digestion, the extracted CO_2 was cryogenically separated from H_2O and other non-condensable gases in a vacuum line using dry ice–ethanol slush and liquid nitrogen. Measurements of carbon and oxygen isotopes were made using Thermoquest DELTA Plus XL coupled with a GasBench II preparation device at Tokyo Institute of Technology (modified after Révész and Landwehr, 2002). Carbon and oxygen isotopic values ($\delta^{13}C$ and $\delta^{18}O$) from carbonate are reported in ‰ relative to the Vienna Peedee Belemnite (VPDB) using the NBS-19 international standard ($\delta^{13}C_{VPDB} = +1.95$ ‰ and $\delta^{18}O_{VPDB} = -2.20$ ‰). The analytical reproducibility of the $\delta^{13}C_{carb}$ and $\delta^{18}O_{carb}$ values is usually better than ±0.3 ‰ and ± 0.5 ‰, respectively. The details of the analytical methods are described elsewhere (Ishikawa et al., 2008).

3.2. REE abundance analysis

Rock powders were dissolved in 2 M acetic acid at 70 °C overnight for REE abundance and strontium isotope analyses. After the insoluble residues were separated from the sample solutions, the dissolved samples were dried and redissolved in 2 M nitric acid. To determine whole-rock REE compositions, an indium solution was added as an internal standard. REE compositions of the solutions were analyzed using inductively coupled plasma-mass spectrometry (ICP-MS; ELEMENT XR, Thermo Scientific) at the University of Tokyo. The sample-standard bracketing technique was employed to improve the reproducibility of the measurements. Two carbonate rock standards, JLs-1 and JDo-1, were also analyzed to verify analytical accuracy (Table S5). Measurement precisions were better than 5 %. In this study, we used the post-Archean average Australian shale (PAAS) composition (Taylor and McLennan, 1985) for normalization of REE contents, as PAAS is commonly used for the normalization of sedimentary rocks (e.g., Bolhar et al., 2004). $[REE]_{PAAS}$ represents the REE content of the sample normalized to that of PAAS. The yttrium anomaly is defined as $[Y]_{PAAS} / [Y^*]_{PAAS}$, where $[Y^*]_{PAAS} = ([Dy]_{PAAS} \times [Ho]PAAS)^{1}/^{2}$. The lanthanum anomaly is defined as $[La]_{PAAS} / [La^*]_{PAAS}$, where $[La^*]_{PAAS} = 3 \times [Pr]_{PAAS} - 2 \times [Nd]_{PAAS}$ (Bolhar et al., 2004). For these parameters, considering analytical error, values higher than 1.1 are considered positive anomalies in this study. The cerium anomaly is defined as $[Ce]_{PAAS} / [Ce^*]_{PAAS}$, where $[Ce^*]_{PAAS} = 2 \times [Pr]_{PAAS} - 1 \times [Nd]_{PAAS}$. The degree of light rare earth element (LREE) and middle rare earth element (MREE) enrichment relative to heavy rare earth element (HREE) is evaluated using $[Pr/Yb]_{PAAS}$ and $[Sm/Yb]_{PAAS}$, respectively.

3.3. Strontium isotopic analysis

Mn, Rb, and Sr abundances were determined using inductively coupled plasma-mass spectrometry (ICP-MS; Agilent 7700, Agilent Technologies) at Gakushuin University. Measurement precisions were better than 3 %. To avoid isobaric interference, Sr was chemically separated from coexisting matrix elements, including Rb, using

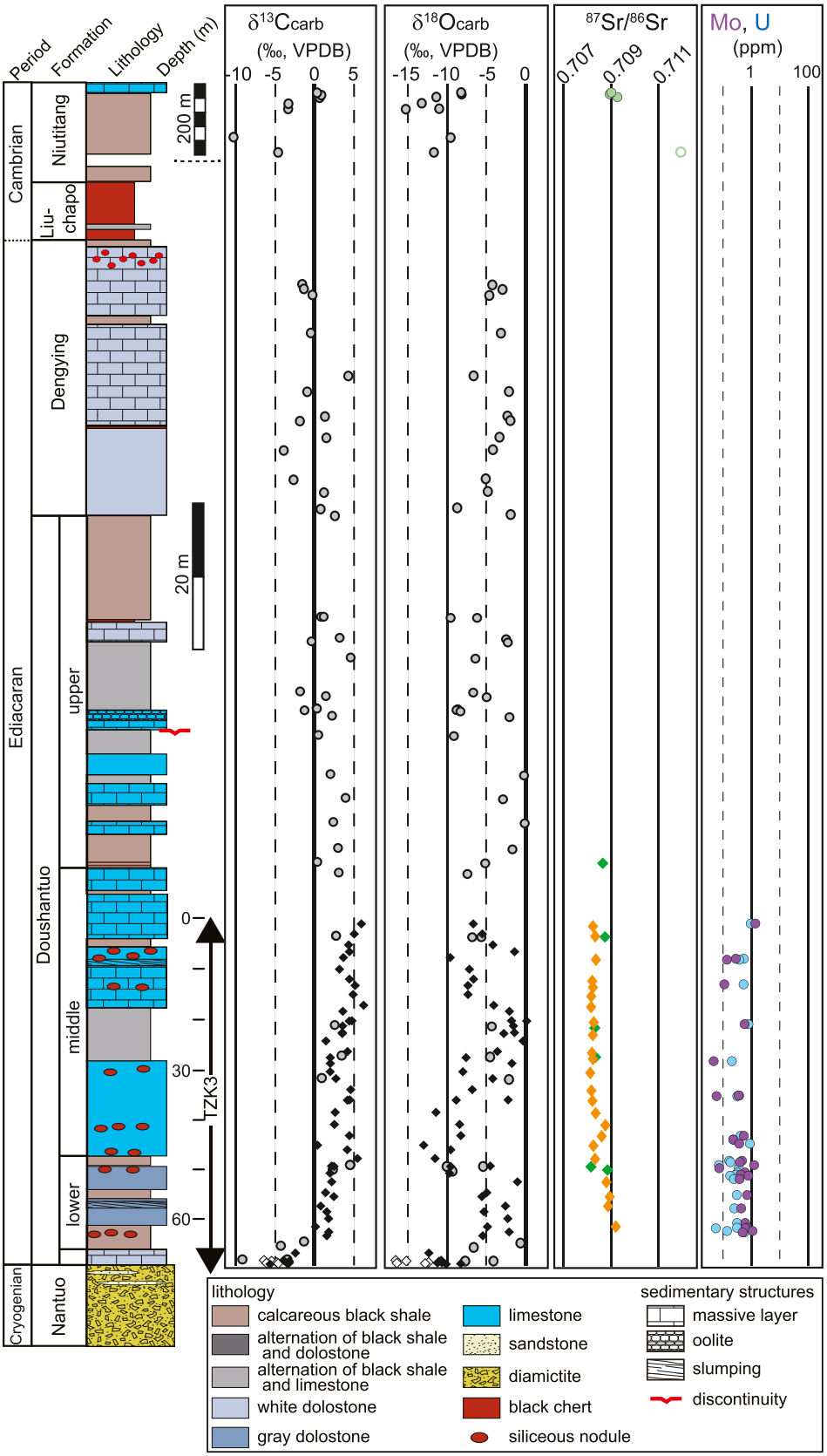

Fig. 3. Lithostratigraphy of the Tianping section from the late Cryogenian through the Ediacaran to the Cambrian. White rhomboids next to cap carbonates represent the isotopic data obtained from veins. Open symbols in the $^{87}Sr/^{86}Sr$ diagram indicate $^{87}Sr/^{86}Sr$ data with Mn/Sr ratios higher than 1 and/or Sr contents lower than 200 μg/g.

chromatographic techniques as described in Ohno and Hirata (2007).

The isotope compositions of ^{86}Sr, ^{87}Sr, and ^{88}Sr were measured using a multi-collector ICP-MS (Nu Plasma 500, Nu Instruments Ltd., Wrexham, Wales) at Gakushuin University. The sample-standard bracketing technique was also employed to improve the analytical reproducibility of the measurements. All $^{87}Sr/^{86}Sr$ isotope ratios were corrected by normalizing the $^{87}Sr/^{86}Sr$ isotope ratio of the standard (NIST SRM 987) to 0.71025. The initial values of radiogenic $^{87}Sr/^{86}Sr$ isotope ratios were calculated from minimum depositional ages, Rb/Sr ratios, and a half-life of ^{87}Rb of 4.88×10^{10} years. A detailed description of the correction of mass discrimination effects is provided elsewhere (Ohno and Hirata, 2007; Ohno et al., 2008).

3.4. Molybdenum and uranium abundance analysis

Rock powders were dissolved in 6 M nitric acid at 100 °C overnight for determination of Mo and U concentrations. Main target of this acid treatment is decomposition of carbonate and pyrite. The temperature and nitric acid concentration are assumed to be enough to completely dissolve pyrite (Kadıoğlu et al., 1995). After the insoluble residues had been excluded from sample solutions, dissolved samples were dried and re-dissolved into 0.5 M nitric acid. After the addition of Indium solution as an internal standard, Mo and U concentrations of the solutions were analyzed using an inductively coupled plasma-mass spectrometry (ICP-MS; ELEMENT XR, Thermo Scientific) at the University of Tokyo. Measurement precisions were better than 5 %. We used JCp-1, JLs-1, and JB-3 standards as secondary standards. The measured

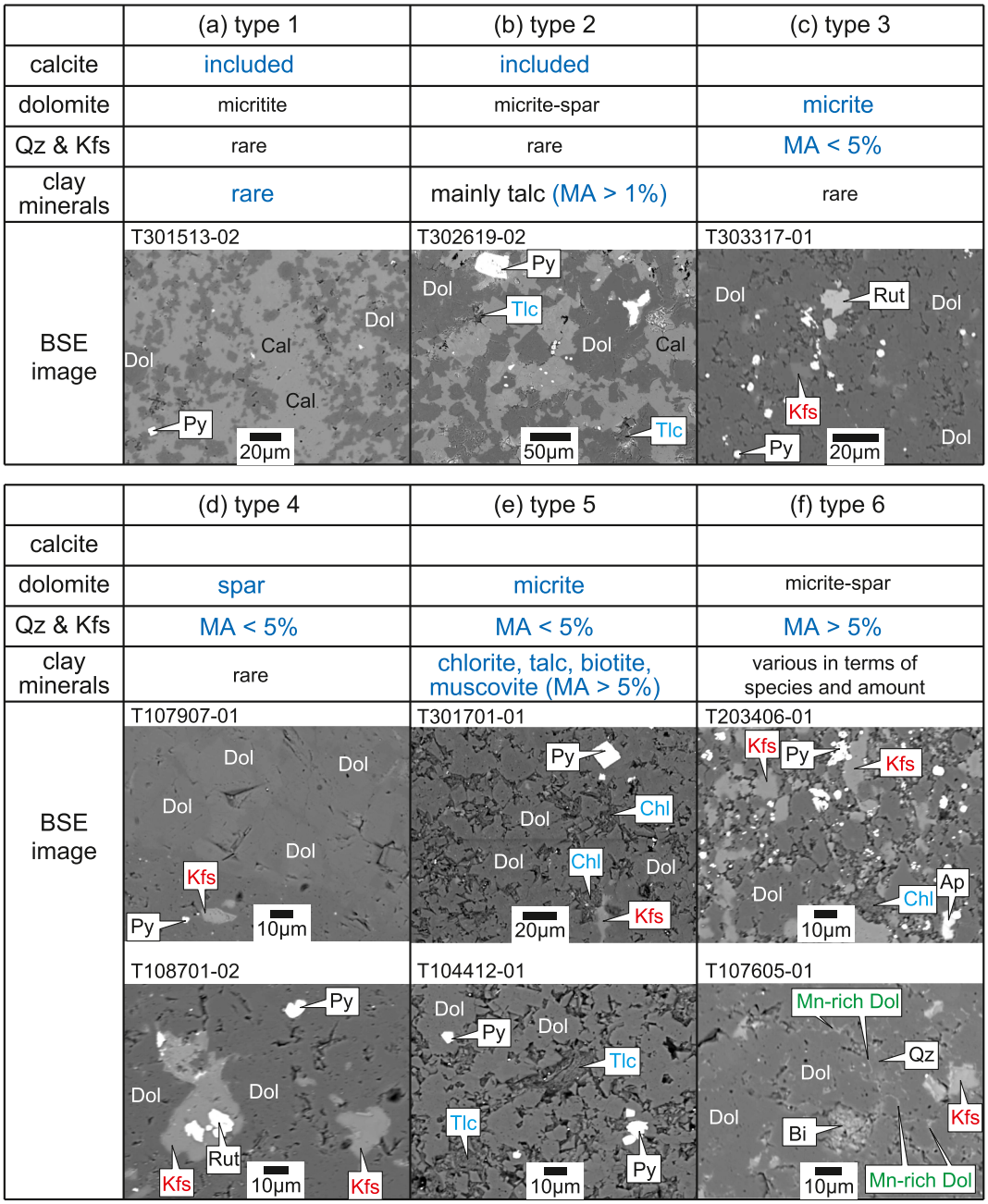

Fig. 4. Backscatter images of analyzed carbonate rocks. Blue-highlighted texts mean definition of each type, whereas black fonts represent characteristics of the type. MA; modal abundance. Ap; apatite. Bi; biotite. Cal; calcite. Chl; chlorite. Dol; dolomite. Kfs; K-feldspar. Py; pyrite. Qz; quartz. Rut; rutile. Tlc; talc. (For interpretation of the references to colour in this figure legend, the reader is referred to the web version of this article.)

concentrations obtained for the secondary standards were, within analytical error, consistent with the referenced values (Table S6).

4. Results

4.1. Sample description

Thin sections were prepared from the collected samples. Dolomite is observed in all analyzed rocks, and calcite is found in some carbonate rocks at the Tianping section. For opaque and clay minerals, we performed mineral identification using a Jeol JSM-6060LV scanning electron microscope (SEM) with an Oxford Instruments INCA X-act energy-dispersive spectrometer (EDS) at the University of Tokyo. Almost all samples contain pyrite grains. Most of the clay minerals were talc, chlorite, muscovite (illite), and biotite. We identified minor amounts of apatite, rutile, hornblende, and detrital plagioclase. Anhedral quartz and K-feldspar filled the gaps between euhedral-subhedral dolomite grains.

Based on the mineralogy, we categorized the analyzed carbonate rocks into six types. Types 1 and 2 are limestone, characterized by the presence of numerous calcite grains (Figs. 4a, b). Most of the dolomite is micritic (<30 μm). Talc was the only clay mineral observed in the limestone samples. The modal abundance of talc in type 1 is lower than 1 %, whereas that in type 2 is greater than 1 %. Types 3–6 were dolostones with few calcite grains. Modal abundances of gap-filling K-feldspar and quartz in types 3–5 are lower than 5 %. Types 3 and 4 dolostones contain minor amounts of clay minerals. Type 3 dolostone is mainly composed of micritic dolomite (Fig. 4c), whereas type 4 dolostone is largely occupied by sparitic (>30 μm) dolomite (Fig. 4d). Under optical microscope observation, type 4 dolostone appears similar to planar-s in Machel (2004). Type 5 dolostone is defined by abundant clay minerals, with a modal abundance greater than 5 % (Fig. 4e). Clay minerals include chlorite, talc, muscovite, and biotite, in descending order of content. Type 6 dolostone is defined by abundant gap-filling K-feldspar and quartz, with a modal abundance greater than 5 % (Figs. 4f, S2). The amounts and types of clay minerals varied for each specimen. The Mn- and Fe-rich dolomite rim occurred at the periphery of dolomite grains, indicating that this rim was formed during late stages of diagenesis.

4.2. Carbon and oxygen isotope ratio

The stratigraphic profile of the $\delta^{13}C$ values of drill-core samples (TZK1 and 2) at the Siduping section shows three negative anomalies (Fig. 2). The $\delta^{13}C$ values in the Cap carbonate range from −3 ‰ to −5 ‰, and the carbon isotopes of the veins tend to be lower than those of the adjacent dolostones (Table S2). $\delta^{13}C$ values continuously increase from −3 ‰ to +5 ‰ in the lower Doushantuo Fm and keep positive values throughout the middle and upper Doushantuo Fm, except for five points at depths of 92.12, 105.06, 108.04, 152.42, and 157.03 m (Table S1). $\delta^{13}C$ values decrease from +5 ‰ to −10 ‰, with minimum $\delta^{13}C$ values being observed at the black shale in the upper Doushantuo Fm. The $\delta^{18}O$ values in the Cap carbonate are scattered between ca. −13 ‰ and − 6 ‰ (Table S2) and are apparently correlated with $\delta^{13}C$ values (Fig. S3a). With the exception of the Cap carbonate, $\delta^{18}O$ values systematically vary throughout the Ediacaran, increasing from −9 ‰ to −3 ‰ in the lower part of the Doushantuo Fm (Fig. 2). Following an abrupt decrease at a depth of ca. 40 m in TZK2, $\delta^{18}O$ values again increase from the middle Doushantuo Fm into the upper Doushantuo Fm, albeit with some anomalously low values. Within the middle and upper Doushantuo Fm, most $\delta^{13}C$ values do not correlate with the corresponding $\delta^{18}O$ values (Figs. 2 and S3a). Negative $\delta^{13}C$ values at depths of 152.42, 156.27, and 157.03 m in TZK1, however, accompany low $\delta^{18}O$ values. Detailed comparison of $\delta^{13}C$ and $\delta^{18}O$ variation with the previous works is described in supplementary items.

4.3. REE content

Fig. 5 illustrates the PAAS-normalized REE patterns of the analyzed samples. Most samples exhibit LREE-enriched and MREE-enriched patterns, as evidenced by $[Pr/Yb]_{PAAS}$ and $[Sm/Yb]_{PAAS}$ values exceeding 1.0 (Fig. 6a). The $[Sm/Yb]_{PAAS}$ value shows no clear correlation with Mn content (Fig. 6b). Some samples display positive La, europium (Eu), and Y anomalies in their REE patterns (Fig. 5). Most data obtained from type 1 limestones show both positive La and Y anomalies (Fig. 6c). The majority of data from types 3 and 4 dolostones exhibit a positive Y anomaly. Conversely, positive Y anomalies are not observed in data from type 2 limestone, types 5 and 6 dolostones. Overall, the Y anomaly shows a slight negative correlation with the Ce anomaly ($R = -0.46$; Fig. 6d).

4.4. Strontium isotope ratio

Because radiogenic strontium isotope ratios are highly susceptible to post-depositional alteration processes, detailed stratigraphic profiles for each section are presented only after a comprehensive evaluation of potential influences from secondary processes (see Section 5.2 for the details). Dolostones in the cap carbonate exhibit extremely high $^{87}Sr/^{86}Sr$ ratios (> 0.7139) and are accompanied by high Mn/Sr ratios (> 15; Fig. 7b). Excluding the cap carbonate, the $^{87}Sr/^{86}Sr$ values of carbonate rocks at the Siduping and Tianping sections ranged from approximately 0.7082 to 0.7129 and from approximately 0.7081 to 0.7092, respectively. Compared with dolostones at the Siduping section, most carbonate rocks at the Tianping section are characterized by high Sr contents and low Mn/Sr ratios (Figs. 7a, b). As a general trend, the $^{87}Sr/^{86}Sr$ value becomes highly scattered when Sr content falls below 200 μg/g (Fig. 7a) or the molar Mn/Sr value exceeds 1.0 (Fig. 7b). The $^{87}Sr/^{86}Sr$ values exhibit no obvious correlations with Rb/Sr ratios (Fig. 7c).

4.5. Molybdenum and uranium contents

Throughout the sequences at Tianping and Siduping sections, Mo and U abundances of most analyzed rocks are below 1 μg/g (Figs. 2, 3, and S4). On the other hand, at the Siduping section, the black shales above the cap carbonate (interval 1) and near top of the Doushantuo Fm (interval 2) are enriched in both Mo and U. The Mo concentration of intervals 1 and 2 ranged within 11–118 μg/g and 151–241 μg/g, respectively.

5. Discussion

5.1. Diagenetic processes

Radiogenic strontium isotopic compositions in carbonate rocks are susceptible to alteration processes. For example, interaction with clay minerals, diagenetic fluids, and meteoric water with high radiogenic isotope ratios can increase their $^{87}Sr/^{86}Sr$ ratios. Therefore, we summarize the diagenetic history that affected the carbonate rocks at the Siduping and Tianping sections.

5.1.1. Dolomitization

All six types of carbonate rocks contain dolomite grains (Fig. 4), indicating that all analyzed rocks experienced some degree of dolomitization (Fig. 8). Thermal convection in open systems involving seawater or slightly modified seawater can form massive sedimentary dolostones (Machel, 2004), where Mg originates from seawater. In this context, Ediacaran carbonate rocks are expected to exhibit a seawater-like REE pattern. Modern seawater and Holocene marine carbonate rocks show positive La, gadolinium (Gd), and Y anomalies and depletion of LREE relative to HREE (Webb and Kamber, 2000; Bolhar et al., 2004). Among these, La and Y anomalies are commonly observed in Phanerozoic limestones (Yoshida et al., 2024). Therefore, we emphasize these two

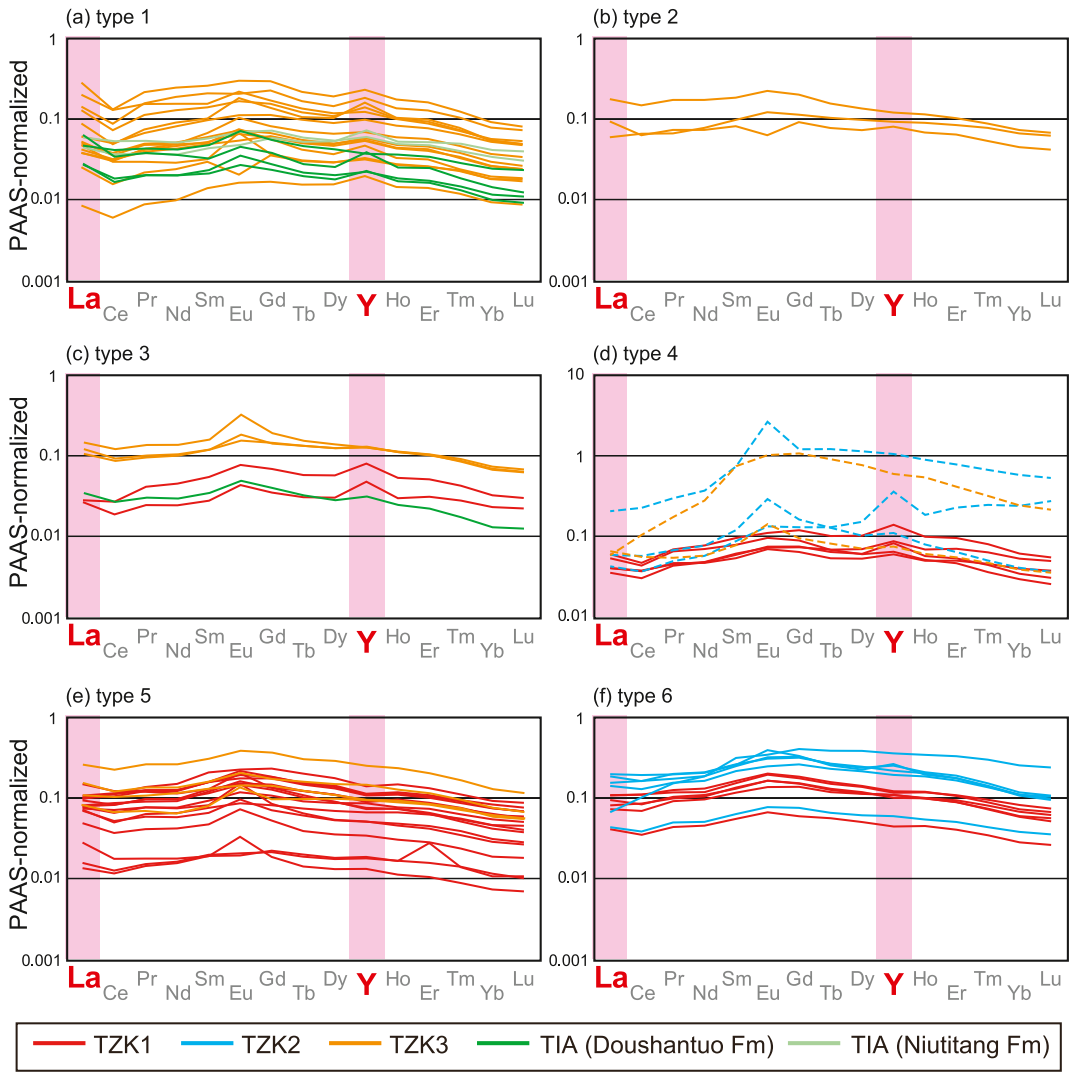

Fig. 5. PAAS-normalized REE patterns for the analyzed samples. Dotted lines in (d) mean data obtained from cap carbonate.

parameters, the presence of which is hereafter referred to as a seawater-like REE pattern. Modern Bahamian dolostones also exhibit positive La and Y anomalies (Liu et al., 2019). However, REE patterns of carbonate rocks can be overprinted by porewater during early diagenesis (Skinner et al., 2019).

Among the six types of carbonate rocks, the REE patterns of type 1 limestones closely resemble those of modern seawater, particularly regarding the presence of positive La and Y anomalies (Fig. 6c). Although the La anomaly is ambiguous, types 3 and 4 dolostones also exhibit a positive Y anomaly. Conversely, positive Y anomalies are obscure in type 2 limestone and types 5 and 6 dolostones. These latter three types of carbonate rocks are characterized by abundant clay minerals (Fig. 4). Clay minerals in these rocks mainly consist of chlorite, talc, muscovite, and biotite, all of which are silicate minerals. These silicates or their precursor detritus were likely supplied from the continental crust or precipitated from slightly modified seawater, causing dolomitization (Fig. 8). Tornos and Spiro (2000) suggested that the reaction between upwelling silica and Mg-rich brines and carbonate rocks leads to both talc mineralization and dolomitization. REE patterns of these components would likely appear flat in PAAS-normalized diagrams. These observations suggest that the inclusion of clay minerals masked the seawater-like positive La and Y anomalies originally recorded in carbonate minerals.

Positive Y anomalies are evident in both type 1 limestone and types 3 and 4 dolostones. German and Elderfield (1990) proposed that only sediments undergoing oxic diagenesis preserve seawater-like REE signatures. A slight negative correlation between Y and Ce anomalies supports this idea (Fig. 6d), although the validity of the Ce anomaly as a redox proxy has recently been questioned by Zhang and Shields (2023). Instead, we consider that the scarcity of detrital clay minerals in types 1, 3, and 4 is more crucial for preserving the seawater-like REE signature. Regardless of the cause, REE patterns in types 3 and 4 dolostones indicate that the fluid causing dolomitization was seawater.

Unlike modern seawater, nearly all carbonate rocks analyzed in this study exhibit MREE-rich patterns (Fig. 5), expressed as high $[Sm/Yb]_{PAAS}$ values (Fig. 6a). Zhang and Shields (2023) also observed similar MREE-rich patterns in Proterozoic carbonate rocks, attributing them to the dissolution of Fe—Mn oxides. Although the correlation between Y anomaly and Mn content is obscure (Fig. 6b), Mn-rich dolomite rims are observed in some dolostones (Figs. 4f, S2). Thus, the dissolution of Fe—Mn oxide phases during diagenesis might contribute to MREE enrichment. Similar to the observations in Zhang and Shields (2023), some carbonate rocks in this study show weak positive Eu anomalies (Fig. 5). Similar weak positive Eu anomalies are also seen in Holocene reefal microbialites (Webb and Kamber, 2000). Experimentally determined partition coefficients of Eu are slightly higher than those of neighboring Sm and Gd (Tanaka and Kawabe, 2006). This might account for the positive Eu anomalies in Ediacaran carbonate rocks.

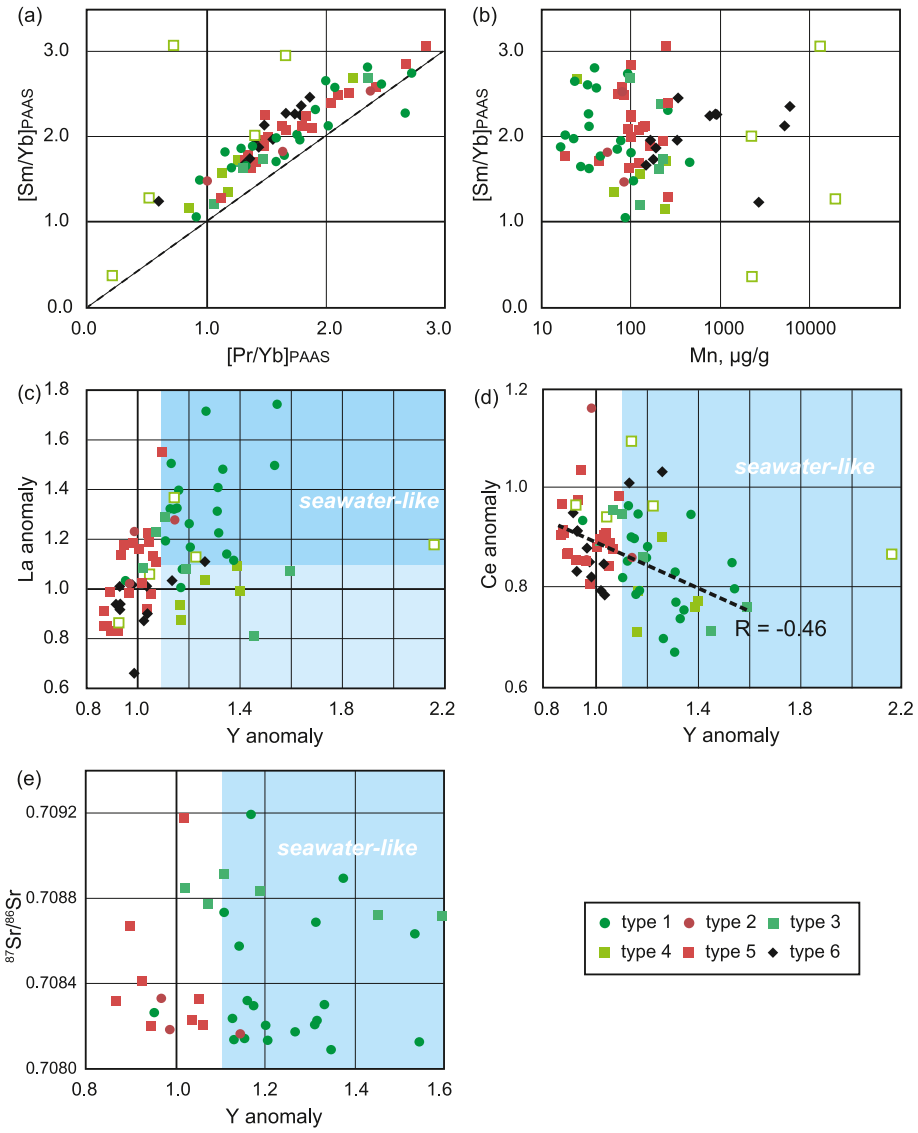

Fig. 6. Crossplots of PAAS-normalized Pr/Yb versus (a) Sm/Yb values (b) Mn content for each type. Identity (1-to-1) line in (a) is dashed. Data above this line mean that MREE are more enriched than LREE. Open squares mean data obtained from cap carbonate. Crossplots of Y anomaly versus (c) La anomaly, (d) Ce anomaly, and (e) $^{87}Sr/^{86}Sr$ of each type.

5.1.2. *Later silicification*

SEM-EDS observations revealed that gaps between dolomite grains are filled with quartz and K-feldspar, particularly noticeable in types 3–6 dolostones (Figs. 4c-f, S2). This indicates that the carbonate rocks underwent silicification after dolomitization. Dolomitization likely increases rock porosity due to the reduction of rock volume (e.g., Weyl, 1960). Porewater penetrating the gaps could precipitate quartz and K-feldspar during later stages of diagenesis.

5.2. *Influence of post-depositional alteration on $^{87}Sr/^{86}Sr$*

The least-altered Ediacaran carbonate rocks in other areas yield $^{87}Sr/^{86}Sr$ ratios lower than 0.7092 (e.g., Halverson et al., 2010; Sawaki et al., 2010a, b). However, some carbonate rocks at the Siduping section exhibit higher $^{87}Sr/^{86}Sr$ ratios, accompanied by high Mn/Sr and Rb/Sr ratios. Therefore, these high Sr isotopic ratios may result from later alteration processes. The carbonate rocks in this study were deposited with detritus and experienced dolomitization and later silicification (Fig. 8). Zhang and Shields (2023) proposed that even if seawater-like REE patterns are masked during early diagenetic processes, the $^{87}Sr/^{86}Sr$ isotope ratios of carbonate rocks could remain unaltered in the absence of significant detritus dissolution.

Previous research has often cited ^{18}O-depletion, low Sr content, and high Mn/Sr and Rb/Sr ratios as indicators of diagenetic alteration (e.g., Banner and Hanson, 1990; Derry et al., 1989; Halverson et al., 2007; Jacobsen and Kaufman, 1999), but threshold values vary among studies (Chen et al., 2022). This likely reflects variations in local sedimentary environments, such as oceanic redox conditions and the chemical composition of coeval seawater. In our dataset, $^{87}Sr/^{86}Sr$ values show significant variation when Sr content falls below 200 μg/g (Fig. 7a) or the molar Mn/Sr value exceeds 1.0 (Fig. 7b). Thus, we tentatively removed $^{87}Sr/^{86}Sr$ data points with low Sr contents (< 200 μg/g) and/or high Mn/Sr ratios (> 1) from the secular trend of $^{87}Sr/^{86}Sr$ value. The $^{87}Sr/^{86}Sr$ data points removed by this criterion are marked by open symbols in Figs. 2 and 3. Previous studies have used Rb/Sr ratios to identify the least-altered and detritus-free samples (Asmerom et al., 1991; Derry et al., 1989; Kaufman et al., 1993), but our dataset shows no clear correlation or trend between $^{87}Sr/^{86}Sr$ and Rb/Sr ratios (Fig. 7c).

Most carbonate rocks at the Tianping section, except for the cap carbonate and TIA123, have high Sr contents and low Mn/Sr ratios

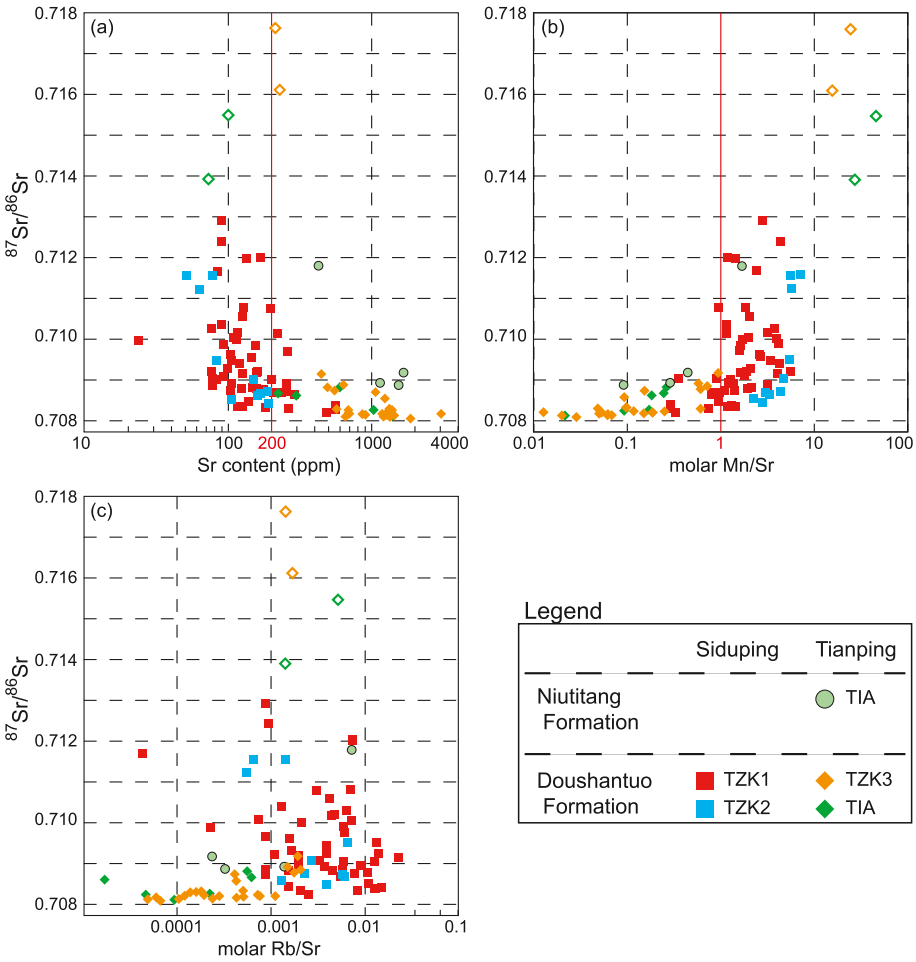

Fig. 7. Isotopic and elemental cross-plots of drill-core samples for $^{87}Sr/^{86}Sr$ versus (a) Sr contents, (b) molar Mn/Sr values, and (c) molar Rb/Sr values.

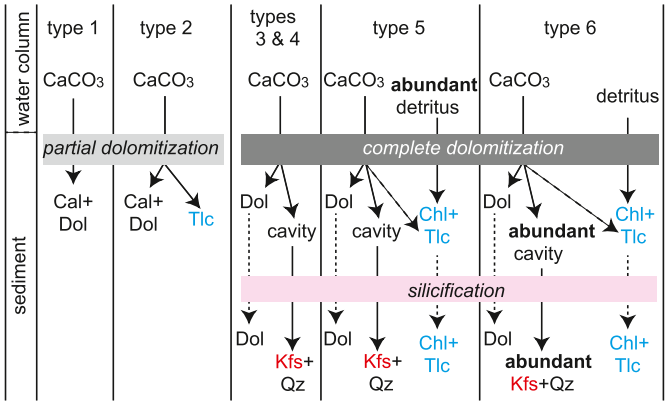

Fig. 8. Schematic diagram showing diagenetic history from which the carbonate rocks at the Siduping and Tianping sections suffered. Cal; calcite. Chl; chlorite. Dol; dolomite. Kfs; K-feldspar. Qz; quartz. Tlc; talc.

(Figs. 7a, b), indicating that the influence of secondary alteration during diagenesis on the $^{87}Sr/^{86}Sr$ ratios of these samples was insignificant. The $^{87}Sr/^{86}Sr$ ratios at the Tianping section show a decreasing smooth curve from approximately 0.7092 just above the cap carbonate to approximately 0.7082 in the middle of the Doushantuo Fm, with a small positive excursion in the lower part (Fig. 3). Subsequently, $^{87}Sr/^{86}Sr$ ratios increased from approximately 0.7086 in the upper Doushantuo Fm to approximately 0.7090 in the Niutitang Fm. In the case of the Siduping section, dolostones characterized by low Sr contents and high Mn/Sr ratios tend to exhibit high $^{87}Sr/^{86}Sr$ ratios (Figs. 7a, b). After removing these data, $^{87}Sr/^{86}Sr$ ratios in the upper Doushantuo Fm approximately ranged from 0.7082 to 0.7087 (Fig. 2).

5.3. Evolution of the $^{87}Sr/^{86}Sr$ composition of ediacaran seawater

Based on the compiled $^{87}Sr/^{86}Sr$ and $\delta^{13}C_{carb}$ values reported from various sections within South China (Fig. 9), we discuss the Ediacaran seawater $^{87}Sr/^{86}Sr$ curve. The residence time of Sr in the Ediacaran ocean was likely longer than the thermohaline ocean circulation (Sawaki et al., 2010a). Therefore, we assume that Ediacaran carbonate rocks share a unique secular trend unless the sedimentary environment experienced hiatus or basin restriction. We define eight intervals based on lithology, $^{87}Sr/^{86}Sr$, and $\delta^{13}C_{carb}$ values (Fig. 9).

5.3.1. Cap carbonate

The Ediacaran $\delta^{13}C_{carb}$ curve in South China starts with a negative excursion in the cap carbonate, and the first Ediacaran negative excursion is called EN1 (Zhou and Xiao, 2007). Cap carbonate samples at the Tianping section exhibit high $^{87}Sr/^{86}Sr$ ratios and extremely high Mn/Sr ratios (Tables S3, S4). These characteristics are common for Marinoan cap carbonates in Namibia (Wang et al., 2023), North China (Wei et al., 2019), Mongolia (Liu et al., 2014), Australia (Liu et al., 2013), Scotland (Sawaki et al., 2010), and Svalbard (Tahata et al., 2015a). Previous studies have suggested that such high $^{87}Sr/^{86}Sr$ ratios in cap carbonate are evidence of transient inputs of terrestrial meltwater and deglacial runoff (Liu et al., 2013, 2014; Wei et al., 2019). However, because most data are accompanied by Mn/Sr ratios higher than 1.0, it is suspected

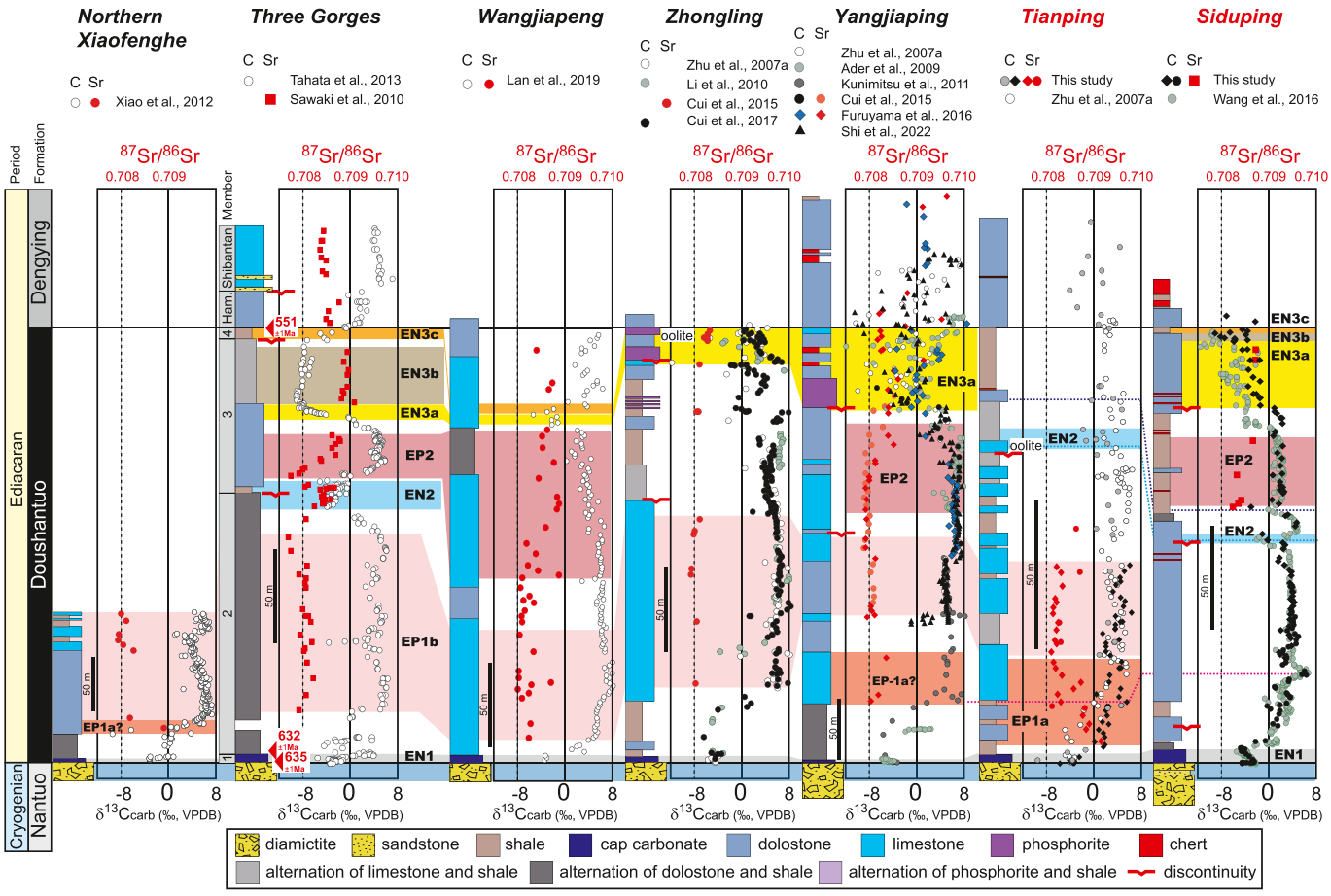

Fig. 9. Comparison of Ediacaran stratigraphic profiles of $\delta^{13}C$ values and $^{87}Sr/^{86}Sr$ ratios within the South China basin (modified after Condon et al., 2005; Ader et al., 2009; Cui et al., 2015, 2017; Furuyama et al., 2016; Kunimitsu et al., 2011; Lan et al., 2019; Li et al., 2010; Sawaki et al., 2010a; Shi et al., 2022; Tahata et al., 2013; Xiao et al., 2012; Wang et al., 2016; Zhu et al., 2007a). Lithology of the Zhongling section is based on Zhu et al. (2007a). Stratigraphic position of discontinuity is based on Jiang et al. (2011). Ham, Hamajing.

that post-depositional processes influenced $^{87}Sr/^{86}Sr$ ratios in cap carbonate. If we apply the same threshold values for Sr content (< 200 μg/g) and molar Mn/Sr value (< 1.0) to identify the least-altered carbonate rocks, five data points reported from Namibia satisfy the criterion. Their $^{87}Sr/^{86}Sr$ ratios ranged from 0.7086 to 0.7089. However, because Wang et al. (2023) considered that the dolostones in Namibia predominantly precipitated from meltwater, it remains uncertain whether the high $^{87}Sr/^{86}Sr$ ratios reflected a global signal.

5.3.2. *Lower Doushantuo Fm*

The lower Doushantuo Formation is characterized by a broad and pronounced positive $\delta^{13}C_{carb}$ excursion (Fig. 9). The first Ediacaran positive excursion is called EP1 (Zhou and Xiao, 2007), and it is subdivided into two parts on the basis of $^{87}Sr/^{86}Sr$ ratio. EP1a corresponds to the interval above the cap carbonate, during which $^{87}Sr/^{86}Sr$ ratios decrease from approximately 0.7092 to approximately 0.7080 and $\delta^{13}C_{carb}$ values increase from 0 ‰ to approximately +5 ‰ (Fig. 9). EP1b is defined by the intervals characterized by constant $^{87}Sr/^{86}Sr$ ratios around 0.7080, where most $\delta^{13}C_{carb}$ values are around +5 ‰. EP1b is evident in various settings, ranging from tidal flat facies to slope facies. In contrast, EP1a is visible only at the Tianping section. Although Xiao et al. (2012) reported an $^{87}Sr/^{86}Sr$ value of 0.7089 above the cap carbonate at the northern Xiaofenghe section, the influence of alteration on their samples has not been tested using other indices. We consider that the lack of EP1a in other sections is attributable to (a) the absence of least-altered carbonate rocks at the Northern Xiaofenghe, Three Gorges, and Zhongling sections, or (b) the scarcity of analyzed $^{87}Sr/^{86}Sr$ data at the Wangjiapeng and Yangjiaping sections for this interval. The combination of high-resolution analysis and the presence of least-altered carbonate rocks at the Tianping section led to the discovery of high $^{87}Sr/^{86}Sr$ ratios preserved in the lower part of the Doushantuo Fm.

Fan et al. (2024) reported $^{87}Sr/^{86}Sr$ values higher than 0.709 from the phosphorites of the Doushantuo Fm at the Weng'an section, attributing these high values to the enhanced contribution of terrigenous materials to the local depositional environment. The Weng'an section was located in a shelf margin setting (Fig. 1). This implies that the sedimentary record at the Weng'an section might not reflect the signature of the open ocean. In contrast, the Tianping section was located in a slope setting, closer to the open ocean. Furthermore, most $^{87}Sr/^{86}Sr$ data from the lower Doushantuo Fm at the Tianping section are classified as type 1 and are accompanied by positive Y anomalies (Fig. 6e), in which carbonate rocks are used as an indicator of deposition in an open marine environment (e.g., Kawabe et al., 1991; Bau, 1996; Webb and Kamber, 2000; Yoshida et al., 2024). These lines of evidence indicate that the $^{87}Sr/^{86}Sr$ compositions of carbonate rocks in the Tianping section are expected to reflect the global change of $^{87}Sr/^{86}Sr$ and that continental weathering influx was elevated during this interval.

During EP1b, $^{87}Sr/^{86}Sr$ ratios are consistently low (around 0.7082) from the shallow marine depositional environments at the northern Xiaofenghe to the continental slopes at the Tianping section (Fig. 9). The aforementioned transient high continental weathering influx was terminated by this interval.

5.3.3. Middle and upper Doushantuo Fm

The middle Doushantuo Formation is characterized by a broad negative $\delta^{13}C_{carb}$ excursion called EN2 and a positive $^{87}Sr/^{86}Sr$ excursion (Fig. 9). A broad positive $\delta^{13}C_{carb}$ excursion occurs in the upper Doushantuo Formation and is called EP2. The interval exhibiting a positive $^{87}Sr/^{86}Sr$ shift. A sharp negative $\delta^{13}C_{carb}$ excursion occurs in the uppermost Doushantuo Formation from inner shelf to slope settings (Fig. S5). This largest negative $\delta^{13}C_{carb}$ anomaly is called the Shuram excursion, EN3, or DOUNCE (DOUshantuo Negative Carbon isotope Excursion; Zhu et al., 2007b). EN3a, EN3b and EN3c represent the decreasing, stable, and recovery intervals of the EN3 excursion, respectively (McFadden et al., 2008). During the EN3a-b interval, $^{87}Sr/^{86}Sr$ ratios are approximately 0.7085 (Fig. 9).

We posit that a negative $\delta^{13}C$ anomaly observed around an oolite layer at the Tianping section corresponds to that observed around the Member 2/3 boundary at the Three Gorges section (EN2 in Fig. 9). Tahata et al. (2013) attributed the negative $\delta^{13}C$ anomaly around the Member 2/3 boundary at the Three Gorges section to the Gaskiers glaciation. The presence of both an oolite layer and regional discontinuity below the oolite indicate that the bathymetry at the Tianping section became shallower than during the deposition of other layers. The relative sea level decrease recorded during the deposition of the oolite layer at the Tianping section also likely attributable to the Gaskiers glaciation. Wang et al. (2016) interpreted a negative $\delta^{13}C$ anomaly in the middle of the Doushantuo Fm at the Siduping section as corresponding to that around the Member 2/3 boundary at the Three Gorges section. A comparative analysis of $\delta^{13}C$ profiles between the Siduping and Tianping sections supports this interpretation (Fig. S6). In general, regional stratigraphic discontinuities have been recognized in the middle Doushantuo Fm (Jiang et al., 2011; Fig. 9). The discontinuities likely explain the lack of EN2 at the Zhongling and Yangjiaping sections. A positive $^{87}Sr/^{86}Sr$ shift and the predominance of positive $\delta^{13}C$ values in the lower portion of Member 3 at the Three Gorges section likely correspond to those in the upper Doushantuo Fm at the Siduping section (EP2 in Fig. 9).

The Shuram excursion, found in Ediacaran shallow marine sediments deposited worldwide (e.g., Burns and Matter, 1993; Fike et al., 2006; Le Guerroué et al., 2006; Melezhik et al., 2009; Tahata et al., 2013, 2015b; Zhu et al., 2013; Furuyama et al., 2017), is accompanied by high $^{87}Sr/^{86}Sr$ ratios ranging from 0.7088 to 0.7091 at the Three Gorges section (EN3b in Fig. 9; Sawaki et al., 2010a). Similar large negative $\delta^{13}C$ anomaly can be seen in the upper Doushantuo Fm at the Wangjiapeng and Zhongling sections (Fig. 9). A negative $\delta^{13}C$ anomaly can be also seen in the upper Doushantuo Fm at the Yanjiaping section. Cui et al. (2015) interpreted the negative $\delta^{13}C$ anomalies at this section as corresponding to the Shuram excursion (EN3), whereas Furuyama et al. (2016) correlated the negative $\delta^{13}C$ values in the upper Doushantuo Formation with EN2 in the Yangtze Gorges area. The latter correlation was based on the $^{87}Sr/^{86}Sr$ values within the uppermost Doushantuo negative $\delta^{13}C$ excursion intervals. However, when $^{87}Sr/^{86}Sr$ data are screened using Sr contents and carbonate contents, the remaining $^{87}Sr/^{86}Sr$ values look similar to those in the EN3 interval (Shi et al., 2022).

At the Siduping section, we consider that the negative $\delta^{13}C$ excursion in the uppermost part of the Doushantuo Fm corresponds to the Shuram excursion (EN3 in Fig. 9), as suggested by Wang et al. (2016) (Fig. S5). Although the data are limited, $^{87}Sr/^{86}Sr$ ratios in this interval at the Siduping section support a high continental weathering rate during the Shuram excursion. During the interval of topmost Doushantuo Fm, the $\delta^{13}C$ values at the Siduping and the Three Gorges sections remained negative (EN3c).

5.4. Implications

5.4.1. Snowball Earth

Whether the Cryogenian global glaciations were a Snowball condition (e.g., Hoffman et al., 1998) or a Slushball condition (Hyde et al., 2000) remains controversial. In addition to model calculations (e.g., Abbot et al., 2011), the cyclicity observed in glacial deposits (Allen and Etienne, 2008) favors the Slushball condition. Song et al. (2023) raised the possibility that habitable open-ocean conditions extended into mid-latitude coastal oceans during the Marinoan glaciation.

As proposed in Li et al. (2020), this argument can be resolved by investigating the intensity of continental weathering after the glaciation. Deglacial intense continental weathering supports the Snowball Earth hypothesis rather than the Slushball Earth hypothesis. To date, a strong influx of terrestrial meltwater has been proposed on the basis of stable isotope signatures obtained from Marinoan cap carbonate (e.g., Kasemann et al., 2005; Wang et al., 2023; Gan et al., 2024). However, the interpretation of stable isotopes is not straightforward, and existing data are not necessarily directly linked to enhanced continental weathering. In this regard, the $^{87}Sr/^{86}Sr$ value of marine carbonate rocks more directly reflects terrestrial weathering influx. Current $^{87}Sr/^{86}Sr$ data obtained from Marinoan cap carbonate rocks have been interpreted as evidence of the addition of terrestrial meltwater (e.g., Liu et al., 2014; Wei et al., 2019). Because this potentially reflects a local and/or short-lived event, we consider that existing data obtained from cap carbonate are not compelling evidence of enhanced continental weathering on a global scale.

The first high $^{87}Sr/^{86}Sr$ value is obtained from the dolostone at approximately 6 m above the cap carbonate (Table S3), indicating that the sequence were temporally distant from the immediate aftermath of the Marinoan glaciation. However, the precipitation of diagnostic "cap" carbonates sitting on top of Cryogenian glacial deposits occurred in <1 Myr (Zhou et al., 2019). The $^{87}Sr/^{86}Sr$ and $\delta^{13}C$ stratigraphic profiles at relatively pelagic settings, such as the Tianping section, potentially enable tracking of $^{87}Sr/^{86}Sr$ changes after the Marinoan glaciation. Because Ediacaran seawater $^{87}Sr/^{86}Sr$ curve shows a decreasing trend from the beginning (Fig. 10), we consider that additional reasons for the enhanced continental weathering other than the Marinoan glaciation are unnecessary. In this context, the high $^{87}Sr/^{86}Sr$ ratios observed in carbonate rocks of the lower Doushantuo Fm at the Tianping section provide supporting evidence for high weathering inputs after Marinoan glaciation, as proposed in the Snowball Earth hypothesis (e.g., Hoffman et al., 1998; Hoffman and Schrag, 2002). Regarding the early Ediacaran, such high $^{87}Sr/^{86}Sr$ ratios are not observed in the Proterozoic seawater $^{87}Sr/^{86}Sr$ curve reconstructed by Chen et al. (2022). This might be attributed to the scarcity of least-altered carbonate rocks of early Ediacaran age.

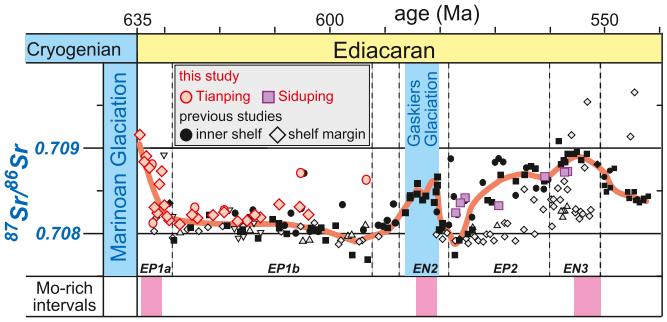

Fig. 10. Reconstructed oceanic $^{87}Sr/^{86}Sr$ changes during the Ediacaran, based on the data presented in Fig. 9. The ages are fixed on following four fixed points; bottom of the Doushantuo Fm (635 Ma), Gaskiers glaciation (ca. 582 Ma), top of the Doushantuo Fm (551 Ma), and Precambrian/Cambrian boundary (539 Ma). Red curve mainly follows data from inner shelf and slope facies, because data from shelf margin are scattered. (For interpretation of the references to colour in this figure legend, the reader is referred to the web version of this article.)

5.4.2. Ocean oxygenation

In the modern oxygenated ocean, euxinic shales in marine basins may better capture the inventory of dissolved redox-sensitive elements in the open ocean (e.g., Algeo and Tribovillard, 2009; Large et al., 2014). Iron speciation and pyrite morphology indicate that most of the Doushantuo Fm at the Wuhe section was deposited under euxinic conditions (Fig. 1; Wang et al., 2012). Based on data from some sections (Gregory et al., 2017; Och et al., 2016; Ostrander et al., 2019; Sahoo et al., 2012, 2016; Tian and Luo, 2017), modern-level Mo enrichments are observed in shale deposited at approximately 635 Ma (basal Member 2), approximately 580 Ma (Member 2/3 boundary), and approximately 560 Ma (Member 4) (Fig. S4). These enrichment events indicate an expanded Mo inventory closely associated with ocean oxygenation events (Sahoo et al., 2016) (Fig. 10). Sawaki et al. (2010a) demonstrated that carbonate rocks around the Member 2/3 boundary and Member 4 exhibit $^{87}Sr/^{86}Sr$ values approaching approximately 0.709 (Fig. 9). This study revealed that the carbonate rocks at basal Member 2 also have such high $^{87}Sr/^{86}Sr$ values (Figs. 3 and 9). Every oxygenation event occurred during an interval of enhanced continental weathering (Fig. 10). This might provide supporting evidence for a close connection between continental weathering and ocean oxygenation.

6. Conclusions

We conducted on-land drilling at the Tianping and Siduping sections to obtain fresh and continuous rock samples deposited during the Ediacaran period. Microscopic observations revealed that the carbonate rocks at these sections experienced dolomitization, clay mineral formation, and silicification. The presence of abundant clay minerals masked seawater-like REE patterns preserved in carbonate phases, whereas data from clay mineral-free carbonate rocks indicated deposition in an open ocean setting. We reported radiogenic strontium isotope profiles in the Ediacaran Doushantuo Formation at these two sections. $^{87}Sr/^{86}Sr$ values in the basal Doushantuo Formation at the Tianping section decreased from 0.7092 to approximately 0.708. This suggests that continental weathering influx was elevated following the Marinoan Snowball Earth event. A compilation of existing data indicates that high $^{87}Sr/^{86}Sr$ ratios around the Shuram excursion were a common feature of carbonate rocks deposited in various settings at that time. The timings of Mo enrichment in euxinic shales coincided with the intervals characterized by high $^{87}Sr/^{86}Sr$ ratios. This supports the hypothesis that globally elevated rates of continental weathering were closely linked to ocean oxygenation events during the Ediacaran.

CRediT authorship contribution statement

Yusuke Sawaki: Visualization, Methodology, Investigation, Funding acquisition, Formal analysis, Data curation, Conceptualization, Writing – original draft. **Kota Namba:** Formal analysis, Data curation. **Takuya Aikawa:** Formal analysis, Data curation. **Miyuki Tahata:** Formal analysis, Data curation. **Takeshi Ohno:** Methodology, Funding acquisition, Formal analysis, Writing – review & editing. **Tsuyoshi Komiya:** Supervision, Resources, Funding acquisition, Conceptualization, Writing – review & editing. **Jian Han:** Investigation, Project administration.

Declaration of competing interest

The authors declare that they have no known competing financial interests or personal relationships that could have appeared to influence the work reported in this paper.

Acknowledgements

This work was mainly supported by a grant from the Ministry of Education, Culture, Sports, Science and Technology, Japan (No. 23340152, No. 23654176, No. 26800259)", the Mitsubishi Foundation, and the Global COE Program "From the Earth to "Earths". We thank Prof. Naohiro Yoshida and Mariko Abe for assistance in the acquisition of analytical data. On-land drilling was performed through the help of Prof. Degan Shu and Dr. Yong Li.

Appendix A. Supplementary data

Supplementary data to this article can be found online at https://doi.org/10.1016/j.palaeo.2025.113270.

Data availability

The authors confirm that all data necessary for supporting the scientific findings of this paper have been provided.

References

Abbot, D.S., Voigt, A., Koll, D., 2011. The Jormungand global climate state and implications for Neoproterozoic glaciations. J. Geophys. Res. Atmos. 116 (D18).
Ader, M., Macouin, M., Trindade, R.I.F., Hadrien, M., Yang, Z.Y., Sun, Z.M., Besse, J., 2009. A multilayered water column in the Ediacaran Yangtze platform? Insights from carbonate and organic matter paired δ13C. Earth Planet. Sci. Lett. 288 (1–2), 213–227.
Algeo, T.J., Tribovillard, N., 2009. Environmental analysis of paleoceanographic systems based on molybdenum–uranium covariation. Chem. Geol. 268 (3–4), 211–225.
Allen, P.A., Etienne, J.L., 2008. Sedimentary challenge to snowball Earth. Nat. Geosci. 1 (12), 817–825.
Asmerom, Y., Jacobsen, S.B., Knoll, A.H., Butterfield, N.J., Swett, K., 1991. Strontium isotopic variations of Neoproterozoic seawater: implications for crustal evolution. Geochim. Cosmochim. Acta 55 (10), 2883–2894.
Banner, J.L., Hanson, G.N., 1990. Calculation of simultaneous isotopic and trace element variations during water-rock interaction with applications to carbonate diagenesis. Geochim. Cosmochim. Acta 54 (11), 3123–3137.
Bau, M., 1996. Controls on the fractionation of isovalent trace elements in magmatic and aqueous systems: evidence from Y/Ho, Zr/Hf, and lanthanide tetrad effect. Contrib. Mineral. Petrol. 123 (3), 323–333.
Bolhar, R., Kamber, B.S., Moorbath, S., Fedo, C.M., Whitehouse, M.J., 2004. Characterisation of early Archaean chemical sediments by trace element signatures. Earth Planet. Sci. Lett. 222 (1), 43–60.
Brasier, M., Antcliffe, J., 2004. Decoding the Ediacaran enigma. Science 305 (5687), 1115–1117.
Bristow, T.F., Kennedy, M.J., Derkowski, A., Droser, M.L., Jiang, G., Creaser, R.A., 2009. Mineralogical constraints on the paleoenvironments of the Ediacaran Doushantuo Formation. Proc. Natl. Acad. Sci. 106 (32), 13190–13195.
Burns, S.J., Matter, A., 1993. Carbon isotopic record of the latest Proterozoic from Oman. Eclogae Geol. Helv. 86 (2), 595–607.
Chen, J.Y., Oliveri, P., Gao, F., Dornbos, S.Q., Li, C.W., Bottjer, D.J., Davidson, E.H., 2002. Precambrian animal life: probable developmental and adult cnidarian forms from Southwest China. Dev. Biol. 248 (1), 182–196.
Chen, L., Xiao, S., Pang, K., Zhou, C., Yuan, X., 2014a. Cell differentiation and germ–soma separation in Ediacaran animal embryo-like fossils. Nature 516 (7530), 238–241.
Chen, Z., Zhou, C., Xiao, S., Wang, W., Guan, C., Hua, H., Yuan, X., 2014b. New Ediacara fossils preserved in marine limestone and their ecological implications. Sci. Rep. 4 (1), 4180.
Chen, X., Zhou, Y., Shields, G.A., 2022. Progress towards an improved Precambrian seawater 87Sr/86Sr curve. Earth Sci. Rev. 224, 103869.
Condon, D., Zhu, M., Bowring, S., Wang, W., Yang, A., Jin, Y., 2005. U-Pb ages from the neoproterozoic Doushantuo Formation, China. Science 308 (5718), 95–98.
Cui, H., Kaufman, A.J., Xiao, S., Zhu, M., Zhou, C., Liu, X.M., 2015. Redox architecture of an Ediacaran Ocean margin: Integrated chemostratigraphic ($\delta^{13}C$–$\delta^{34}S$–$^{87}Sr/^{86}Sr$–Ce/Ce*) correlation of the Doushantuo Formation, South China. Chem. Geol. 405, 48–62.
Cui, H., Kaufman, A.J., Xiao, S., Zhou, C., Liu, X.M., 2017. Was the Ediacaran Shuram Excursion a globally synchronized early diagenetic event? Insights from methane-derived authigenic carbonates in the uppermost Doushantuo Formation, South China. Chem. Geol. 450, 59–80.
Cui, H., Kitajima, K., Orland, I.J., Xiao, S., Baele, J.M., Kaufman, A.J., Denny, A., Zhou, C., Spicuzza, M.J., Fournelle, J.H., Valley, J.W., 2021. Deposition or diagenesis? Probing the Ediacaran Shuram excursion in South China by SIMS. Glob. Planet. Chang. 206, 103591.
Dalziel, I.W., 1991. Pacific margins of Laurentia and East Antarctica-Australia as a conjugate rift pair: evidence and implications for an Eocambrian supercontinent. Geology 19 (6), 598–601.
Derry, L.A., Keto, L.S., Jacobsen, S.B., Knoll, A.H., Swett, K., 1989. Sr isotopic variations in Upper Proterozoic carbonates from Svalbard and East Greenland. Geochim. Cosmochim. Acta 53 (9), 2331–2339.
Des Marais, D.J., 1994. Tectonic control of the crustal organic carbon reservoir during the Precambrian. Chem. Geol. 114 (3–4), 303–314.

Fan, H., Zhang, H., Wei, W., Hiatt, E.E., Ward, J.F., Wen, H., 2024. Phosphorus flux during the Ediacaran: Rooted in continental weathering or pelagic upwelling? Earth Planet. Sci. Lett. 646, 118975.
Fike, D.A., Grotzinger, J.P., Pratt, L.M., Summons, R.E., 2006. Oxidation of the Ediacaran ocean. Nature 444 (7120), 744–747.
Furuyama, S., Kano, A., Kunimitsu, Y., Ishikawa, T., Wang, W., 2016. Diagenetic overprint to a negative carbon isotope anomaly associated with the Gaskiers glaciation of the Ediacaran Doushantuo Formation in South China. Precambrian Res. 276, 110–122.
Furuyama, S., Kano, A., Kunimitsu, Y., Ishikawa, T., Wang, W., Liu, X.C., 2017. Chemostratigraphy of the Ediacaran basinal setting on the Yangtze platform, South China: Oceanographic and diagenetic aspects of the carbon isotopic depth gradient. Island Arc 26 (5), e12196.
Gan, T., Tian, M., Wang, X.K., Wang, S., Liu, X.M., Jiang, G., Gill, B.C., Nolan, M., Kaufman, A.J., Luo, T., Xiao, S., 2024. Lithium isotope evidence for a plumeworld ocean in the aftermath of the Marinoan snowball Earth. Proceedings of the National Academy of Sciences 121 (46), e2407419121.
Garrels, R.M., Perry, E.A., 1974. Cycling of carbon, sulfur, and oxygen through geologic time. Sea 5, 303–336.
German, C.R., Elderfield, H., 1990. Application of the Ce anomaly as a paleoredox indicator: the ground rules. Paleoceanography 5 (5), 823–833.
Gregory, D.D., Lyons, T.W., Large, R.R., Jiang, G., Stepanov, A.S., Diamond, C.W., Figueroa, M.C., Olin, P., 2017. Whole rock and discrete pyrite geochemistry as complementary tracers of ancient ocean chemistry: an example from the Neoproterozoic Doushantuo Formation, China. Geochim. Cosmochim. Acta 216, 201–220.
Halverson, G.P., Dudás, F.Ö., Maloof, A.C., Bowring, S.A., 2007. Evolution of the $^{87}Sr/^{86}Sr$ composition of Neoproterozoic seawater. Palaeogeogr. Palaeoclimatol. Palaeoecol. 256 (3–4), 103–129.
Halverson, G.P., Wade, B.P., Hurtgen, M.T., Barovich, K.M., 2010. Neoproterozoic chemostratigraphy. Precambrian Res. 182 (4), 337–350.
Hardisty, D.S., Lu, Z., Bekker, A., Diamond, C.W., Gill, B.C., Jiang, G., Kah, L.C., Knoll, A. H., Loyd, S.J., Osburn, M.R., Planavsky, N.J., Wang, C., Zhou, X., Lyons, T.W., 2017. Perspectives on Proterozoic surface ocean redox from iodine contents in ancient and recent carbonate. Earth Planet. Sci. Lett. 463, 159–170.
Hawkins, A.D., Xiao, S., Jiang, G., Wang, X., Shi, X., 2017. New biostratigraphic and chemostratigraphic data from the Ediacaran Doushantuo Formation in intra-shelf and upper slope facies of the Yangtze platform: Implications for biozonation of acanthomorphic acritarchs in South China. Precambrian Res. 300, 28–39.
Hoffman, P.F., Schrag, D.P., 2002. The snowball Earth hypothesis: testing the limits of global change. Terra Nova 14 (3), 129–155.
Hoffman, P.F., Kaufman, A.J., Halverson, G.P., Schrag, D.P., 1998. A Neoproterozoic snowball earth. Science 281 (5381), 1342–1346.
Huang, K.J., Teng, F.Z., Shen, B., Xiao, S., Lang, X., Ma, H.R., Fu, Y., Peng, Y., 2016. Episode of intense chemical weathering during the termination of the 635 Ma Marinoan glaciation. Proc. Natl. Acad. Sci. 113 (52), 14904–14909.
Hurtgen, M.T., Arthur, M.A., Suits, N.S., Kaufman, A.J., 2002. The sulfur isotopic composition of Neoproterozoic seawater sulfate: implications for a snowball Earth? Earth Planet. Sci. Lett. 203 (1), 413–429.
Hyde, W.T., Crowley, T.J., Baum, S.K., Peltier, W.R., 2000. Neoproterozoic 'snowball Earth'simulations with a coupled climate/ice-sheet model. Nature 405 (6785), 425–429.
Ishikawa, T., Ueno, Y., Komiya, T., Sawaki, Y., Han, J., Shu, D., Li, Y., Maruyama, S., Yoshida, N., 2008. Carbon isotope chemostratigraphy of a Precambrian/Cambrian boundary section in the three Gorge area, South China: Prominent global-scale isotope excursions just before the Cambrian Explosion. Gondwana Res. 14, 193–208.
Jacobsen, S.B., Kaufman, A.J., 1999. The Sr, C and O isotopic evolution of Neoproterozoic seawater. Chem. Geol. 161 (1–3), 37–57.
Jiang, G., Kennedy, M.J., Christie-Blick, N., 2003. Stable isotopic evidence for methane seeps in Neoproterozoic postglacial cap carbonates. Nature 426 (6968), 822–826.
Jiang, G., Kaufman, A.J., Christie-Blick, N., Zhang, S., Wu, H., 2007. Carbon isotope variability across the Ediacaran Yangtze platform in South China: Implications for a large surface-to-deep ocean δ13C gradient. Earth Planet. Sci. Lett. 261 (1–2), 303–320.
Jiang, G., Shi, X., Zhang, S., Wang, Y., Xiao, S., 2011. Stratigraphy and paleogeography of the Ediacaran Doushantuo Formation (ca. 635–551 Ma) in South China. Gondwana Res. 19 (4), 831–849.
Kadıoğlu, Y.Y., Karaca, S., Bayrakceken, S., 1995. Kinetics of pyrite oxidation in aqueous suspension by nitric acid. Fuel Process. Technol. 41 (3), 273–287.
Karlstrom, K.E., Åhäll, K.I., Harlan, S.S., Williams, M.L., McLelland, J., Geissman, J.W., 2001. Long-lived (1.8–1.0 Ga) convergent orogen in southern Laurentia, its extensions to Australia and Baltica, and implications for refining Rodinia. Precambrian Res. 111 (1–4), 5–30.
Kasemann, S.A., Hawkesworth, C.J., Prave, A.R., Fallick, A.E., Pearson, P.N., 2005. Boron and calcium isotope composition in Neoproterozoic carbonate rocks from Namibia: evidence for extreme environmental change. Earth Planet. Sci. Lett. 231 (1–2), 73–86.
Kaufman, A.J., Jacobsen, S.B., Knoll, A.H., 1993. The Vendian record of Sr and C isotopic variations in seawater: implications for tectonics and paleoclimate. Earth Planet. Sci. Lett. 120 (3–4), 409–430.
Kawabe, I., Kitahara, Y., Naito, K., 1991. Non-chondritic yttrium/holmium ratio and lanthanide tetrad effect observed in pre-Cenozoic limestones. Geochem. J. 25 (1), 31–44.
Kunimitsu, Y., Setsuda, Y., Furuyama, S., Wang, W., Kano, A., 2011. Ediacaran chemostratigraphy and paleoceanography at a shallow marine setting in northwestern Hunan Province, South China. Precambrian Res. 191 (3–4), 194–208.
Lan, Z., Sano, Y., Yahagi, T., Tanaka, K., Shirai, K., Papineau, D., Sawaki, Y., Ohno, T., Abe, M., Yang, H., Liu, H., Jiang, T., Wang, T., 2019. An integrated chemostratigraphic ($\delta^{13}C$-$\delta^{18}O$-$^{87}Sr/^{86}Sr$-$\delta^{15}N$) study of the Doushantuo Formation in western Hubei Province, South China. Precambrian Res. 320, 232–252.
Large, R.R., Halpin, J.A., Danyushevsky, L.V., Maslennikov, V.V., Bull, S.W., Long, J.A., Gregory, D.D., Lounejeva, E., Lyons, T.W., Sack, P.J., McGoldrick, P.J., Calver, C.R., 2014. Trace element content of sedimentary pyrite as a new proxy for deep-time ocean–atmosphere evolution. Earth and Planetary Science Letters 389, 209–220.
Le Guerroué, E., Allen, P.A., Cozzi, A., 2006. Chemostratigraphic and sedimentological framework of the largest negative carbon isotopic excursion in Earth history: the Neoproterozoic Shuram Formation (Nafun Group, Oman). Precambrian Res. 146 (1–2), 68–92.
Li, Z.X., Li, X.H., Kinny, P.D., Wang, J., 1999. The breakup of Rodinia: did it start with a mantle plume beneath South China? Earth Planet. Sci. Lett. 173 (3), 171–181.
Li, C., Love, G.D., Lyons, T.W., Fike, D.A., Sessions, A.L., Chu, X., 2010. A stratified redox model for the Ediacaran Ocean. Science 328 (5974), 80–83.
Li, J., Hao, C., Wang, Z., Dong, L., Wang, Y., Huang, K.J., Lang, X., Huang, T., Yuan, H., Zhou, C., Shen, B., 2020. Continental weathering intensity during the termination of the Marinoan Snowball Earth: Mg isotope evidence from the basal Doushantuo cap carbonate in South China. Palaeogeogr. Palaeoclimatol. Palaeoecol. 552, 109774.
Liu, C., Wang, Z., Raub, T.D., 2013. Geochemical constraints on the origin of Marinoan cap dolostones from Nuccaleena Formation, South Australia. Chem. Geol. 351, 95–104.
Liu, C., Wang, Z., Raub, T.D., Macdonald, F.A., Evans, D.A., 2014. Neoproterozoic cap-dolostone deposition in stratified glacial meltwater plume. Earth Planet. Sci. Lett. 404, 22–32.
Liu, X.M., Hardisty, D.S., Lyons, T.W., Swart, P.K., 2019. Evaluating the fidelity of the cerium paleoredox tracer during variable carbonate diagenesis on the Great Bahamas Bank. Geochim. Cosmochim. Acta 248, 25–42.
Machel, H.G., 2004. Concepts and models of dolomitization: a critical reappraisal. Geol. Soc. Lond. Spec. Publ. 235, 7–63.
McFadden, K.A., Huang, J., Chu, X., Jiang, G., Kaufman, A.J., Zhou, C., Yuan, X., Xiao, S., 2008. Pulsed oxidation and biological evolution in the Ediacaran Doushantuo Formation. Proc. Natl. Acad. Sci. 105 (9), 3197–3202.
Melezhik, V.A., Pokrovsky, B.G., Fallick, A.E., Kuznetsov, A.B., Bujakaite, M.I., 2009. Constraints on $^{87}Sr/^{86}Sr$ of late Ediacaran seawater: insight from Siberian high-Sr limestones. J. Geol. Soc. Lond. 166 (1), 183–191.
Och, L.M., Cremonese, L., Shields-Zhou, G.A., Poulton, S.W., Struck, U., Ling, H., Li, D., Chen, X., Manning, C., Thirlwall, M., Strauss, H., Zhu, M., 2016. Palaeoceanographic controls on spatial redox distribution over the Yangtze Platform during the Ediacaran–Cambrian transition. Sedimentology 63 (2), 378–410.
Ohno, T., Hirata, T., 2007. Simultaneous determination of mass-dependent isotopic fractionation and radiogenic isotope variation of strontium in geochemical samples by multiple collector-ICP-mass spectrometry. Anal. Sci. 23 (11), 1275–1280.
Ohno, T., Komiya, T., Ueno, Y., Hirata, T., Maruyama, S., 2008. Determination of $^{88}Sr/^{86}Sr$ mass-dependent isotopic fractionation and radiogenic isotope variation of $^{87}Sr/^{86}Sr$ in the Neoproterozoic Doushantuo Formation. Gondwana Res. 14 (1–2), 126–133.
Ostrander, C.M., Sahoo, S.K., Kendall, B., Jiang, G., Planavsky, N.J., Lyons, T.W., Nielsen, S.G., Owens, J.D., Gordon, G.W., Romaniello, S.J., Anbar, A.D., 2019. Multiple negative molybdenum isotope excursions in the Doushantuo Formation (South China) fingerprint complex redox-related processes in the Ediacaran Nanhua Basin. Geochim. Cosmochim. Acta 261, 191–209.
Révész, K.M., Landwehr, J.M., 2002. $\delta^{13}C$ and $\delta^{18}O$ isotopic composition of $CaCO_3$ measured by continuous flow isotope ratio mass spectrometry: statistical evaluation and verification by application to Devils Hole core DH-11 calcite. Rapid Commun. Mass Spectrom. 16, 2102–2114.
Richter, F.M., Rowley, D.B., DePaolo, D.J., 1992. Sr isotope evolution of seawater: the role of tectonics. Earth Planet. Sci. Lett. 109 (1–2), 11–23.
Sahoo, S.K., Planavsky, N.J., Kendall, B., Wang, X., Shi, X., Scott, C., Anbar, A.D., Lyons, T.W., Jiang, G., 2012. Ocean oxygenation in the wake of the Marinoan glaciation. Nature 489 (7417), 546–549.
Sahoo, S.K., Planavsky, N.J., Jiang, G., Kendall, B., Owens, J.D., Wang, X., Shi, X., Anbar, A.D., Lyons, T.W., 2016. Oceanic oxygenation events in the anoxic Ediacaran Ocean. Geobiology 14 (5), 457–468.
Sawaki, Y., Kawai, T., Shibuya, T., Tahata, M., Omori, S., Komiya, T., Yoshida, N., Ohno, T., Windley, B.F., Maruyama, S., 2010. $^{87}Sr/^{86}Sr$ chemostratigraphy of Neoproterozoic Dalradian carbonates below the Port Askaig glaciogenic Formation, Scotland. Precambrian Res. 179 (1–4), 150–164.
Sawaki, Y., Ohno, T., Tahata, M., Komiya, T., Hirata, T., Maruyama, S., Windley, B.F., Han, J., Shu, D., Li, Y., 2010a. The Ediacaran radiogenic Sr isotope excursion in the Doushantuo Formation in the three Gorges area, South China. Precambrian Res. 176 (1–4), 46–64.
Shi, H., Ouyang, Q., Zhou, C., Xiao, S., Chen, Z., Guan, C., 2022. Integrated study of the Doushantuo Formation in northwestern Hunan Province: implications for Ediacaran chemostratigraphy and biostratigraphy in South China. Precambrian Res. 377, 106699.
Shields, G.A., 2005. Neoproterozoic cap carbonates: a critical appraisal of existing models and the plumeworld hypothesis. Terra Nova 17 (4), 299–310.
Skinner, L.C., Sadekov, A., Brandon, M., Greaves, M., Plancherel, Y., de La Fuente, M., Gottschalk, G., Souanef-Uretta, S., Sevilgen, D.S., Scrivner, A.E., 2019. Rare Earth elements in early-diagenetic foraminifer 'coatings': Pore-water controls and potential palaeoceanographic applications. Geochim. Cosmochim. Acta 245, 118–132.
Song, H., An, Z., Ye, Q., Stüeken, E.E., Li, J., Hu, J., Algeo, T.J., Tian, L., Chu, D., Song, H., Xiao, S., Tong, J., 2023. Mid-latitudinal habitable environment for marine

eukaryotes during the waning stage of the Marinoan snowball glaciation. Nat. Commun. 14 (1), 1564.
Squire, R.J., Campbell, I.H., Allen, C.M., Wilson, C.J., 2006. Did the Transgondwanan Supermountain trigger the explosive radiation of animals on Earth? Earth Planet. Sci. Lett. 250 (1–2), 116–133.
Tahata, M., Ueno, Y., Ishikawa, T., Sawaki, Y., Murakami, K., Han, J., Shu, D., Li, Y., Guo, J., Yoshida, N., Komiya, T., 2013. Carbon and oxygen isotope chemostratigraphies of the Yangtze platform, South China: decoding temperature and environmental changes through the Ediacaran. Gondwana Res. 23 (1), 333–353.
Tahata, M., Sawaki, Y., Yoshiya, K., Nishizawa, M., Komiya, T., Hirata, T., Yoshida, N., Maruyama, S., Windley, B.F., 2015a. The marine environments encompassing the Neoproterozoic glaciations: evidence from C, Sr and Fe isotope ratios in the Hecla Hoek Supergroup in Svalbard. Precambrian Res. 263, 19–42.
Tahata, M., Sawaki, Y., Ueno, Y., Nishizawa, M., Yoshida, N., Ebisuzaki, T., Komiya, T., Maruyama, S., 2015b. Three-step modernization of the ocean: Modeling of carbon cycles and the revolution of ecological systems in the Ediacaran/Cambrian periods. Geosci. Front. 6 (1), 121–136.
Tanaka, K., Kawabe, I., 2006. REE abundances in ancient seawater inferred from marine limestone and experimental REE partition coefficients between calcite and aqueous solution. Geochemical Journal 40 (5), 425–435.
Taylor, S.R., McLennan, S.M., 1985. The Continental Crust: Its Composition and Evolution. Blackwell, Oxford, p. 312.
Tian, X., Luo, K., 2017. Distribution and enrichment patterns of selenium in the Ediacaran and early Cambrian strata in the Yangtze Gorges area, South China. Sci. China Earth Sci. 60, 1268–1282.
Tornos, F., Spiro, B.F., 2000. The geology and isotope geochemistry of the talc deposits of Puebla de Lillo (Cantabrian Zone, Northern Spain). Econ. Geol. 95 (6), 1277–1296.
Vernhet, E., Heubeck, C., Zhu, M.Y., Zhang, J.M., 2006. Large-scale slope instability at the southern margin of the Ediacaran Yangtze platform (Hunan province, Central China). Precambrian Res. 148 (1–2), 32–44.
Wachter, E.A., Hayes, J.M., 1985. Exchange of oxygen isotopes in carbon dioxide-phosporic acid systems. Chem. Geol.: Isot. Geosci. Secti. 52, 365–374.
Wang, J., Li, Z.X., 2003. History of Neoproterozoic rift basins in South China: implications for Rodinia break-up. Precambrian Res. 122 (1–4), 141–158.
Wang, L., Shi, X., Jiang, G., 2012. Pyrite morphology and redox fluctuations recorded in the Ediacaran Doushantuo Formation. Palaeogeogr. Palaeoclimatol. Palaeoecol. 333, 218–227.
Wang, X., Jiang, G., Shi, X., Xiao, S., 2016. Paired carbonate and organic carbon isotope variations of the Ediacaran Doushantuo Formation from an upper slope section at Siduping, South China. Precambrian Res. 273, 53–66.
Wang, J., Jacobson, A.D., Sageman, B.B., Hurtgen, M.T., 2023. Application of the $\delta^{44/40}$Ca-$\delta^{88/86}$Sr multi-proxy to Namibian Marinoan cap carbonates. Geochim. Cosmochim. Acta 353, 13–27.
Webb, G.E., Kamber, B.S., 2000. Rare earth elements in Holocene reefal microbialites: a new shallow seawater proxy. Geochim. Cosmochim. Acta 64 (9), 1557–1565.
Wei, G.Y., Hood, A., Chen, X., Li, D., Wei, W., Wen, B., Gong, Z., Yang, T., Zhang, Z.F., Ling, H.F., 2019. Ca and Sr isotope constraints on the formation of the Marinoan cap dolostones. Earth Planet. Sci. Lett. 511, 202–212.
Weyl, P.K., 1960. Porosity through dolomitization–Conservation-of-mass requirements. J. Sediment. Res. 30 (1), 85–90.
Xiao, S., Zhang, Y., Knoll, A.H., 1998. Three-dimensional preservation of algae and animal embryos in a Neoproterozoic phosphorite. Nature 391 (6667), 553–558.
Xiao, S., McFadden, K.A., Peek, S., Kaufman, A.J., Zhou, C., Jiang, G., Hu, J., 2012. Integrated chemostratigraphy of the Doushantuo Formation at the northern Xiaofenghe section (Yangtze Gorges, South China) and its implication for Ediacaran stratigraphic correlation and ocean redox models. Precambrian Res. 192, 125–141.
Xiao, S., Muscente, A.D., Chen, L., Zhou, C., Schiffbauer, J.D., Wood, A.D., Polys, N.F., Yuan, X., 2014a. The Weng'an biota and the Ediacaran radiation of multicellular eukaryotes. Natl. Sci. Rev. 1 (4), 498–520.
Xiao, S., Zhou, C., Liu, P., Wang, D., Yuan, X., 2014b. Phosphatized acanthomorphic acritarchs and related microfossils from the Ediacaran Doushantuo Formation at Weng'an (South China) and their implications for biostratigraphic correlation. J. Paleontol. 88 (1), 1–67.
Yin, L., Zhu, M., Knoll, A.H., Yuan, X., Zhang, J., Hu, J., 2007. Doushantuo embryos preserved inside diapause egg cysts. Nature 446 (7136), 661–663.
Yoshida, S., Mayika, K.B., Ishihara, Y., Moussavou, M., Asanuma, H., Sato, T., Hirata, T., Linga, C., Sawaki, Y., Edou-Minko, A., 2024. Depositional condition of Paleoproterozoic Francevillian carbonate rocks revisited from rare earth element contents. Geosci. Front. 15 (3), 101771.
Zhang, K., Shields, G.A., 2023. Early diagenetic mobilization of rare earth elements and implications for the Ce anomaly as a redox proxy. Chem. Geol. 635, 121619.
Zhao, Z., Xing, Y., Ding, Q., Liu, G., Zhao, Y., Zhang, S., Meng, X., Yin, C., Ning, B., Han, P., 1988. The Sinian System of Hubei. China University of Geosciences Press, Wuhan, p. 205.
Zhou, C., Xiao, S., 2007. Ediacaran δ^{13}C chemostratigraphy of South China. Chem. Geol. 237 (1–2), 89–108.
Zhou, C., Huyskens, M.H., Lang, X., Xiao, S., Yin, Q.Z., 2019. Calibrating the terminations of Cryogenian global glaciations. Geology 47 (3), 251–254.
Zhu, M., Zhang, J., Yang, A., Li, G., Steiner, M., Erdtmann, B.D., 2003. Sinian-Cambrian stratigraphic framework for shallow-to deep-water environments of the Yangtze Platform: an integrated approach. Prog. Nat. Sci. 13 (12), 951–960.
Zhu, M., Zhang, J., Yang, A., 2007a. Integrated ediacaran (sinian) chronostratigraphy of South China. Palaeogeogr. Palaeoclimatol. Palaeoecol. 254 (1–2), 7–61.
Zhu, M., Strauss, H., Shields, G.A., 2007b. From snowball earth to the Cambrian bioradiation: calibration of Ediacaran–Cambrian earth history in South China. Palaeogeogr. Palaeoclimatol. Palaeoecol. 254 (1–2), 1–6.
Zhu, M., Lu, M., Zhang, J., Zhao, F., Li, G., Aihua, Y., Zhao, M., 2013. Carbon isotope chemostratigraphy and sedimentary facies evolution of the Ediacaran Doushantuo Formation in western Hubei, South China. Precambrian Res. 225, 7–28.